

2013

The Effects of Nickel Chloride Stress on Freshwater Cyanobacterium *Synechococcus* SP. IU 625

Brian Nohomovich
Seton Hall University

Follow this and additional works at: <https://scholarship.shu.edu/dissertations>

Part of the [Biology Commons](#)

Recommended Citation

Nohomovich, Brian, "The Effects of Nickel Chloride Stress on Freshwater Cyanobacterium *Synechococcus* SP. IU 625" (2013). *Seton Hall University Dissertations and Theses (ETDs)*. 1883.
<https://scholarship.shu.edu/dissertations/1883>

**THE EFFECTS OF NICKEL CHLORIDE STRESS ON FRESHWATER
CYANOBACTERIUM *SYNECHOCOCCUS* SP. IU 625**

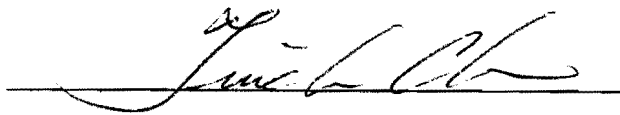
BY

BRIAN NOHOMOVICH

Submitted in partial fulfillment of the requirements for the
degree of Master of Science in Biology from the
Department of Biological Sciences of Seton Hall University

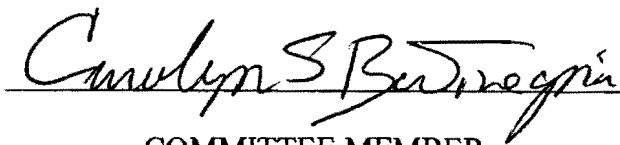
May 2013

APPROVED BY



MENTOR

Dr. Tin-Chun Chu



COMMITTEE MEMBER

Dr. Carolyn Bentivegna



COMMITTEE MEMBER

Dr. David Sabatino



DIRECTOR OF GRADUATE STUDIES

Dr. Allan Blake



CHAIR, DEPARTMENT OF BIOLOGICAL SCIENCES

Dr. Jane Ko

Acknowledgment

Dr. Chu, thank you for all the advice, support, and for providing much needed assistance through our busy schedules.

To my committee, I would like to thank you for reviewing this work and providing much needed feedback.

I am very grateful to Michael Quintanilla and Naturex for performing the ICP-MS work. Your hard work provided a key part of this data.

Finally I extend gratitude to Robert Newby for helping me when I needed it, the Biology Department, and Seton Hall University for making this project possible.

Table of Contents

Introduction	1
Materials and Methods	4
Results	9
Conclusion & Discussion	34
Work Cited	39

List of Figures

Figure 1	Growth Curves of <i>S. IU 625</i> with or without Nickel Stress	13
Figure 2	Pigment Visualization	14
Figure 3	Microscopic Observations of <i>S. IU 625</i> with Various Nickel Concentrations at Day 13	15
Figure 4	Cell Viability under Nickel Exposure throughout the Course of the Study	16
Figure 5	Distribution of Nickel during the growth of <i>S. IU 625</i>	17
Figure 6	Relative Quantification of <i>smtA</i>	23
Figure 7a	Partial Order Alignment (POA) of CnrB	24
Figure 7b	Phylogenetic Analysis of CnrB in <i>Synechococcus</i>	25
Figure 8a	Partial Order Alignment (POA) of AcrB	26
Figure 8b	Phylogenetic Analysis of AcrB in <i>Synechococcus</i>	27
Figure 9a	<i>Synechococcus</i> Species used for POA Analysis	28
Figure 9b	Partial Order Alignment (POA) of CnrB and AcrB	29
Figure 9c	Phylogenetic Analysis of CnrB and AcrB	30
Figure 10	Partial order Alignment (POA) of <i>hylD</i>	31
Figure 11	Potential <i>nsr</i> Operon	32
Figure 12	Potential <i>hae</i> Operon	33

Abstract

The ability of cyanobacteria to grow in heavy metal polluted areas is proving a challenge to environmental restoration initiatives. Cyanobacteria secrete toxins, such as microcystins that are potentially dangerous to human health. Thus, it is an imperative to investigate the cyanobacteria response against heavy metals to gain insight into their remarkable stress response. Understanding this stress response may someday provide insight into combating the algal blooms formed from high densities of cyanobacteria or perhaps means to cure heavy metal polluted areas. By understanding the way cyanobacteria can thrive in these environments, strategies can be developed to counteract them.

To further develop an understanding of the stress response, the physiology of cyanobacteria was assessed to nickel exposure. Cultures were grown in increasing concentrations of nickel chloride. Cell morphology was assessed through microscopy. Cell counts and turbidity provided insight into cell growth. ICP-MS examined the movement of nickel ions within the cell to the outside of the cell through the course of the environment. qPCR of a known heavy metal response gene, *smtA*, provides analysis of potential response mechanism. Finally, bioinformatic analyses provide an understanding of the observed ICP-MS data by highlighting potential nickel response proteins based on homology and phylogeny, as well as the possible resistance mechanism of nickel stress in freshwater cyanobacteria.

Introduction

The formation of algal blooms is a serious concern worldwide for human and animal health. Algal blooms cause oxygen depletion in the aquatic environment. Algal blooms form from the increase use of pesticides, fertilizer, and waste (Brand 2010). The nutrient-enriched environments cause a dramatic increase in the cyanobacteria population and a subsequent decrease in other competing bacteria. The cyanobacteria will then become the dominant population in the aquatic environment. Many species of cyanobacteria secrete toxic metabolites (Banack 2010, Brand 2010). For example, the toxin Beta-N-Methylamino-L-Alanine (BMAA) has been linked to various diseases and is considered a factor in Alzheimer's disease (Banack 2010). Monitoring of global water bodies has become a human health imperative. The way cyanobacteria manage to thrive in heavy metal polluted environments needs to be further evaluated.

The freshwater bacterium, *Synechococcus* sp. IU 625 (*S. IU 625*) is a unicellular rod-shaped microorganism with a similar cell wall structure to Gram-negative bacteria (Chu 2012). *S. IU 625* is an ideal candidate to study heavy metal response mechanisms due to its fast growth, easy maintenance/cultural conditions, and strong homology with two fully sequenced genomes, *Synechococcus elongatus* PCC 7942 (*Syn. PCC 7942*) and *Synechococcus elongatus* PCC 6301 (*Syn. PCC 6301*) (Chu 2012). The unique nature of cyanobacteria to grow in a wide range of environmental conditions makes it an ideal model. Using *S. IU 625* as a model, many biological processes can be assessed including cell cycle, membrane transport and various molecular mechanisms. The use of genome amplification allows for a way to monitor cellular response to a heavy metal stress.

Metallothionein (MT) is a heavy metal stress response protein. *smtA* is the gene that encodes MT. The gene *smtB* encodes a repressor that blocks the transcription of *smtA* (Chu 2007). Binding of heavy metal ions to the repressor exposes the *smtA* binding site allowing for transcription to proceed (Turner 1996). Metallothionein sequesters free heavy metal divalent cations. MT will then be expelled from the cell containing the heavy metals. It has been previously demonstrated that increase expression of MT can increase cell survival in a heavy metal stress environment. Metallothionein has been shown to confer an increased resistance to cadmium, zinc, mercury, and copper (Chu 2007). Previous studies have shown that increasing concentrations of heavy metals can slow cell growth (Lee 1996). Expanding on the previous work, nickel was chosen as a heavy metal stress.

Nickel is an essential metal that plays an important role in health of eukaryotes and prokaryotes (Rodionov 2006). Nickel is a necessary cofactor for enzymatic function in prokaryotes (Rodionov 2006, Zhang 2009). Nickel-associated enzymes play a crucial role in maintaining the global cycle for nitrogen, carbon, and oxygen (Zhang 2009). However, high concentrations of nickel exposure could be potentially toxic. Nickel has been shown to cause detrimental damage to lung tissue (Tchou-Wong 2011, Zhou 2009) and is categorized as a potential carcinogen (Tchou-Wong 2011). It is also a target analyte for the Environmental Protection Agency (EPA). In human cell lines, nickel accumulates intracellularly and effects DNA methylation and iron-uptake systems resulting in iron deficiency. Nickel can impair gene expression levels through an

epigenetic mechanism by increasing the number of DNA methylations present on promoter regions (Tcho-Wong 2011, Zhou 2009).

Cyanobacteria and other prokaryotes can directly be damaged by nickel as well. Nickel can target or interfere with important enzymes involved in photosynthesis (Boisvert 2007, Hemlata 2009). The mechanism of this damage is still undefined but it is thought that nickel acts as free-radical initiator which induces severe damage to the photosystem (Boisvert 2007). Nickel can also bind to the cell wall of the bacteria inducing stress (Lee 1996). Binding of nickel to the cell wall is a biosorption mechanism which has been proposed as a means to clean polluted areas (Gardea-Torresdey 1998, Azeez 1991). The damaging effects of nickel have allowed prokaryotes to develop a wide range of survival methods.

The primary methods in which prokaryotes combat stress are through an efflux protein (Ettinger 2005), a sequestering metal chelate such as metallothionein (Garcia-Domingues 2000, Turner 1996), formation of biofilms as seen in *E. coli* (Perrin 2009) or to turn the harmful heavy metal ion into a neutral molecule. Previous work has shown that *S. IU 625* sequesters or utilizes an efflux mechanism to maintain homeostasis of heavy metal (Chu 2012, Lee 1996). This study provides insight into the effects nickel has on *S. IU 625* and the response it utilizes to reduce nickel toxicity. The gene *smtA* which has been shown to increase heavy metal resistance was monitored exclusively.

Materials and Methods

Cultures Maintenance

S. IU 625 stock cultures were maintained in an Amerex Instruments Inc., (Lafayette, CA), Gyromax 747R incubator shaker at 26 °C in atmospheric conditions with constant fluorescent light and continuous agitation at 100 rpm. Five ml of cells were inoculated in 95 ml of sterilized Mauro's Modified Medium (3M) in 250 mL Erlenmeyer flasks. The media was adjusted to a pH of 7.9 using 1 M NaOH.

Nickel Chloride Preparation

Stock solution of 1% nickel chloride in dH₂O was prepared using triple distilled water Milli-Q Integral 5 Water Purification System (EMD Millipore, MA) in a sterile container from Sigma Aldrich. The solution was then sterilized by using Millipore 0.45 µm membrane filters.

Growth of *Synechococcus* sp. IU 625 in Nickel Chloride

Various nickel chloride concentrations (0, 10, 25, 50 mg/L) was added to an exponentially growing culture in four 250 mL Erlenmeyer flasks, respectively. Cell growth was monitored through; 1) direct counts via hemacytometer, cells were counted in triplicate for each time point and an average of cell number/square was obtained. The

average was then multiplied by 25 and then 10^4 to obtain the cell number per mL; and 2) turbidity study, optical density (OD) was taken by using a Pharmacia LKB Ultraspec III spectrophotometer at 750 nm wavelength. Cell growth was monitored for 28 days with mean and standard deviations generated through GraphPad Prism.

Microscopic Observation

Aliquots of cells (1 mL) were taken from each time point and used for microscopic analyses. Cells were immediately centrifuged for 1 minute and the supernatant was discarded. Cells were fixed using 5X fixative (12.5% formaldehyde in phosphate buffer). DNA was detected with the use of DAPI (4,6-diamidion-2-phenylindole) fluorescence. Cells were incubated with DAPI (2 $\mu\text{g}/\text{mL}$) for 10 minutes in the dark and placed onto a 1% agarose pad that was pre-made on the slide. Cell morphology was observed using differential contrast with on an Axioscope Lab A1 microscope with Zeiss AxioVision software.

DNA Extraction

Flasks 1-3 were overgrown and needed to be diluted for efficient DNA isolation. Flasks 1, 2, 3 were diluted 1:4 with 1x Tris-EDTA (TE) buffer. Culture 4 was not diluted (1:1). The Norgen protocol kit was followed with the change to incubate at 45 minutes for cell lysis due to thickness of some of the samples. The purity (260/280 ratio) and the

yield (ng/ μ L) of the DNA samples were determined with the Thermo Scientific NanoDrop ND-1000.

Heavy Metal Distribution

Samples were centrifuged immediately after collection and the supernatant placed into a separate microcentrifuge tube. The cell pellet was resuspended in dH₂O. The amount of nickel present in the supernatant and in the cells was determined using ICP-MS protocol by Naturex on an ELAN DRC-E ICP-MS.

Naturex ICP-MS Protocol

Standard Solution Generation

Standard solutions were first generated. The matrix solution was prepared with 20% nitric acid (SCP Science – Nitric Acid, PP, 66-70%, Poly- #250-038-175), 500 ppb gold, 50 ppb internal standard. In a clean squeeze bottle, 300 mL of water was added with 100 mL of nitric acid. 0.25 mL of a gold solution (0.25 mL of 1000 ppm gold solution in 10% HCL) (#N9300212) was added to the nitric acid solution. A multi-element internal standard (2.5 mL of 26 element, 100 mg/L, nitric acid) (#N9303834) was subsequently added to the mixture and diluted with water (SCP Science Blank Water for ICP #140-113-037) to 500 mL. A nickel standard, Perkin Elmer Quality Control Standard 21, (#N9300281) was also used to assess the quantity of nickel.

ICP-MS Acid Digestion

A small aliquot of the sample (0.25 g) was weighed directly in microwavable reactor and nitric acid (10 mL) was slowly added. The solution was cooled by capping and mineralizing. A mineralization sequence was followed (see below). After mineralization, the reaction was cooled to 45 °C and transferred to a 50 mL volumetric flask. A mixture of gold: internal standard (275 µL, 1:1) was added. The flask was then diluted with water (50 mL) and filtered into another 50 mL tube.

ICP Operating Conditions

All basic maintenance was followed before turning on; system was allowed to warm for 15 minutes with the hood and argon flow conditions checked

The following setup was used for an ICP-MS Elan DRC-e, Perkin Elmer with autosampler S10, Perkin Elmer. Microwave accelerated Reaction System, Model (MARSr) with 12 digestion reactors XP1500+ vessel Assembly kits. Power: 1.1 kW, Plasma flow: 15 L/min, Auxiliary flow: 0.95 L/min, Nebulizer flow: 0.93 L/min, Wash time between sample: 45 s, Sample delay: 35 s, Dwell timer per mass: 50 ms, Sweeps per reading: 20, Replicates: 3/Reading per replicate: 1

ICP-MS Sample Analysis

A new dataset was generated by placing blanks, standards and samples into the autosampler. After the samples were generated, the tubing was removed, plasma and argon was turned off. The calibration curve was set according to the following

correlation coefficient limit: 0.995, Curve type: linear, Maximum error %: 15, unit for standards: mg/L or after weight ppm.

RNA Isolation, cDNA Synthesis and qPCR

RNA was extracted from the sample using Trizol Max Bacterial RNA Isolation Kit, Invitrogen. Cells were lysed and RNA separated using phase separation and precipitated out of solution to isolate RNA. RNA was stored in nuclease-free dH₂O. RNA quality and concentration was estimated using a NanoDrop ND-1000.

cDNA was generated using a High Capacity Reverse Transcriptase cDNA kit from Applied Biosystems®. Reactions (10 µL) were conducted with 2 µL buffer (10x), 0.8 µL dNTPs, 2.0 µL RT primers, 1.0 µL RT, and 3.2 µL nuclease-free dH₂O. Reactions were placed on the Applied Biosystems® Veriti® 96-Well Thermal Cycler and followed manufacturer recommendations.

Quantitative PCR (qPCR) was performed with an Applied Biosystems® StepOnePlus Real-Time PCR System. Reactions were set up in triplicate with 6.6 µL nuclease-free water, 1.2 µL each of forward and reverse primer (300 nm) for *smtA*, 10 µL of SYBR green dye, and 1 µL of cDNA (5 ng/µL).

Bioinformatic Analyses

Sequences of known efflux proteins CnrB and AcrB were blasted with BlastP separately against *Synechococcus* species. *Syn.* PCC 7942 and *Syn.* PCC 6301 were found within each BlastP and aligned with a survey of other *Synechococcus* species from the results. A multiple sequence alignment was performed with Muscle5, T-Coffee and Partial Order Alignment (POA). A neighbor-joining phylogenetic tree was generated from the Muscle5 alignments. A conserved sequence region was visualized with Partial Order Alignment Visualizer (POAVIZ).

Results

Growth and Pigmentation Defects

To determine the effects of nickel on the growth of *S.* IU 625 cultures were grown in 3M broth with increasing concentrations of nickel, 0, 10, 25 and 50 mg/L. Previous work has established that these concentrations induce the greatest effect for observation. Cultures were monitored twice a week for 3-4 weeks to demonstrate the complete bacteria growth cycle of lag, log and stationary phases. The growth curves demonstrate that an increase in nickel concentration shows a depression in cell growth up until a certain critical nickel concentration threshold. The 10 mg/L culture was only slightly slower than control initially but quickly rebounded. The 25 mg/L culture had a prolonged lag phase and did not fully enter exponential growth until day 11. The total cell count for the 25 mg/L remained lower than the control and 10 mg/L. The 50 mg/L culture showed little growth and the culture color was pale to clear by the end of the study. A pale color indicates the reduction of cell population or the cells lose

pigmentation. Preliminary data (not shown) establishes that the maximal nickel concentration cells can survive in is lower than 30 mg/L. A study with 30 mg/L culture followed the same trend as the 50 mg/L culture.

A lighter pigmentation of green in the 25 mg/L culture was noted from day 1 to day 8, see figure 2. However the cell number increased slightly in the 25 mg/L during this time, see figure 1. An increase in cell number should darken the green coloring, as seen in the 10 mg/L and 0 mg/L culture. It has been documented that nickel ions can interfere with the electron transfer in the photosystem lowering the fluorescence (Boisvert 2007). This suggests an explanation for the bleaching effect seen in the 25 mg/L during its prolonged lag phase. Further, it may account for the relatively flat Optical Density (OD) change present in the growth curve as pigmentation damage would not fluorescence accordingly.

S. IU 625 Morphological Defects

Increasing concentrations of nickel chloride induced more pronounced morphological defects. Defects present include DNA fragmentation, vibrio shaped cells, and cell size changes. The 10 mg/L nickel chloride culture had an increase in curved cells and cells with ectopic poles, as shown in figure 2. After a week these defects declined rapidly and the cells appeared to have normal morphology and intact DNA similar to that of the control. Higher concentration of NiCl₂ showed similar morphological defects to those observed in the 10 mg/L but were more frequently noted. The 25 mg/L cultures developed morphological defects including abnormal cell morphology and fragmented

DNA. More dead cells (as shown by the lack of DNA) were more frequently present in the 25 mg/L culture than that of the 10 mg/L. After 11 days the cells were capable of growing in the 25 mg/L culture with some minor defects such as vibrio morphology, which remained present throughout the rest of the study. The 50 mg/L culture had an increased prevalence in dead cells and appeared smaller in size. This decrease in size could be in part due to a response to minimize surface area to the hostile environment or a decrease in nutrient intake. By the end of the study, the clear flask color and microscopic observations suggest that a significant portion of cells in the 50 mg/L culture were dead. Figure 3 demonstrates some of the common defects and Figure 4 represents the % cell viability. To calculate the % cell viability, a ratio of dead to alive cells was taken for each respective time-point. Live cells had minimal morphological defects and could be stained with DAPI. Cells that were otherwise considered dead did not stain with DAPI and did not fluoresce under UV light.

Nickel Accumulates Initially within *S. IU 625* but is Virtually Cleared by Day 11

ICP-MS provided data for nickel concentrations in the supernatant and within the cells. Nickel concentrations were normalized against the control. The 10 mg/L culture accumulated 8% more nickel in the cell by day 6 and by day 11 it was reduced to control levels. The 25 mg/L culture accumulated less nickel by day 6 (6%) compared to the 10 mg/L culture. However, the 25 mg/L culture was not fully capable of clearing all the nickel into the supernatant throughout the time-points tested. A 1% increase in nickel concentration was always seen in the 25 mg/L culture over control (figure 5).

Cell Aggregation

Some strains of bacteria such as *E. coli* form biofilms (Perrin 2009). Preliminary data suggests that the portions of the 25 mg/L culture and to a lesser extent the 10 mg/L did aggregate together. Cell aggregation perhaps would minimize the cell's exposure to the environment and increase survivability. Further analysis of cellular aggregation is necessary to verify and determine the exact mechanism.

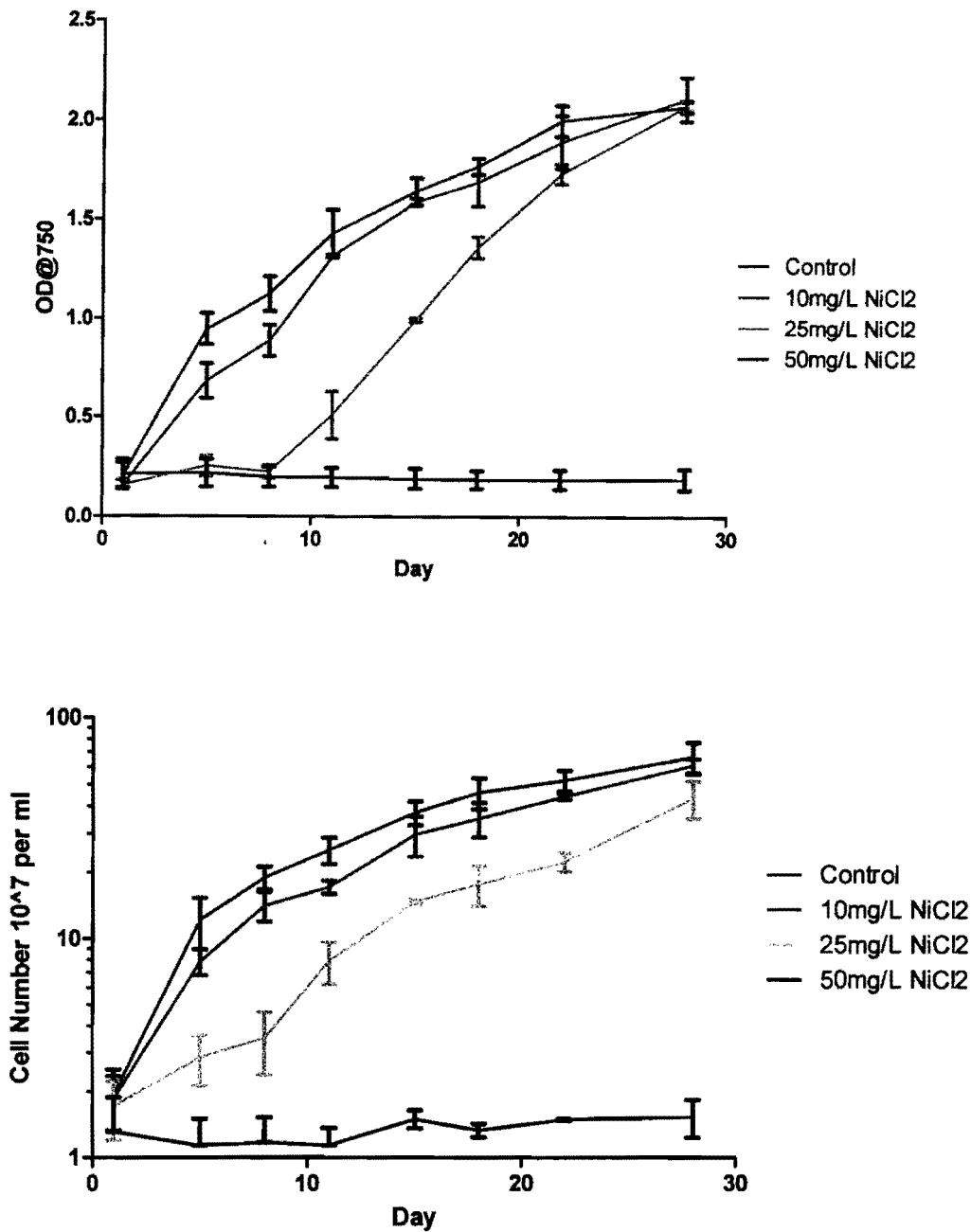


Fig. 1. Growth Curves of *S. IU 625* with or without Nickel Stress: 0 (control), 10, 25 and 50 mg/L NiCl₂, respectively. Triplicate cultures growth curves were plotted using GraphPad Prism. a) Turbidity study with optical density of each culture plotted over the time course in days. b) Direct count of cultures.

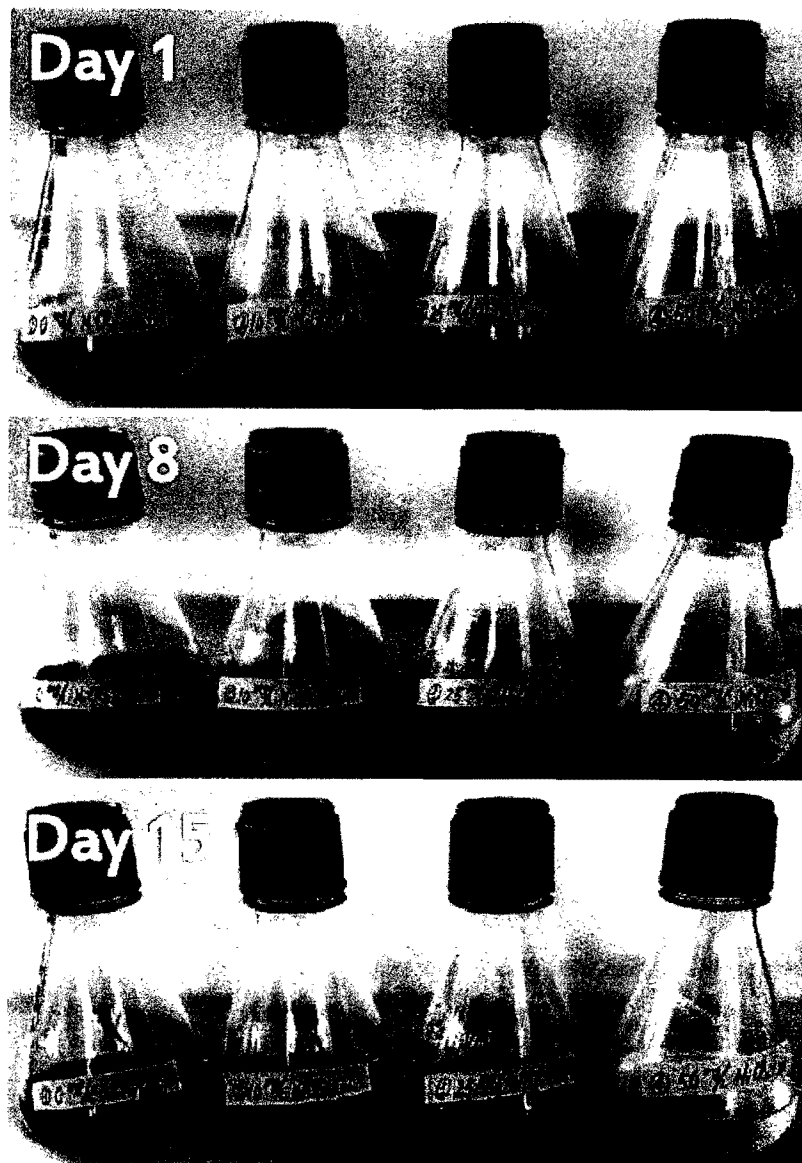


Fig. 2. Pigment Visualization. Left to Right; 0, 10, 25, and 50 mg/L, note the slight discoloration of the 25 mg/L culture on day 8. The color change might be due to free radical nickel ions damaging the pigments. Pictures of flasks were taken each week. Associated day into study is noted in the top left of each picture.

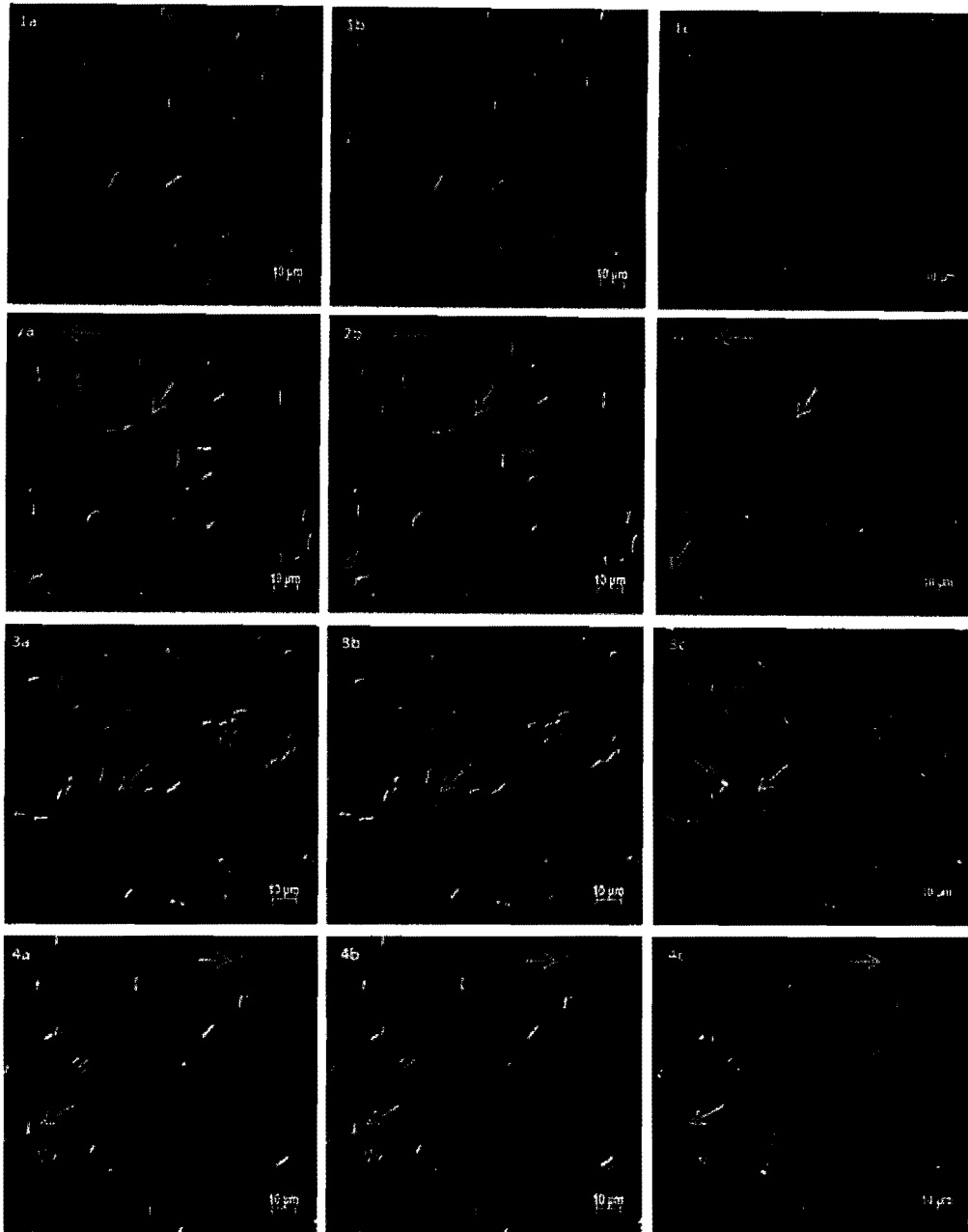


Fig. 3. Microscopic Observations of *S. IU 625* with Various Nickel Concentrations at Day 13. a: overlaid image; b: DIC images; c: DAPI-stained images. 1a-1c: 0 mg/L NiCl₂ (control); 2a-2c: 10 mg/L NiCl₂; 3a-3c: 25 mg/L NiCl₂; 4a-4c: 50 mg/L NiCl₂. Arrows indicate different morphological defects. The same colored arrow indicates the same defect within the culture. Green arrow: normal size cell with no DNA, considered dead; Red arrow: elongated cell may contain DNA; Orange arrow: abnormal morphology, may contain DNA; Purple arrow: Cocci-like, smaller cells, DNA present.

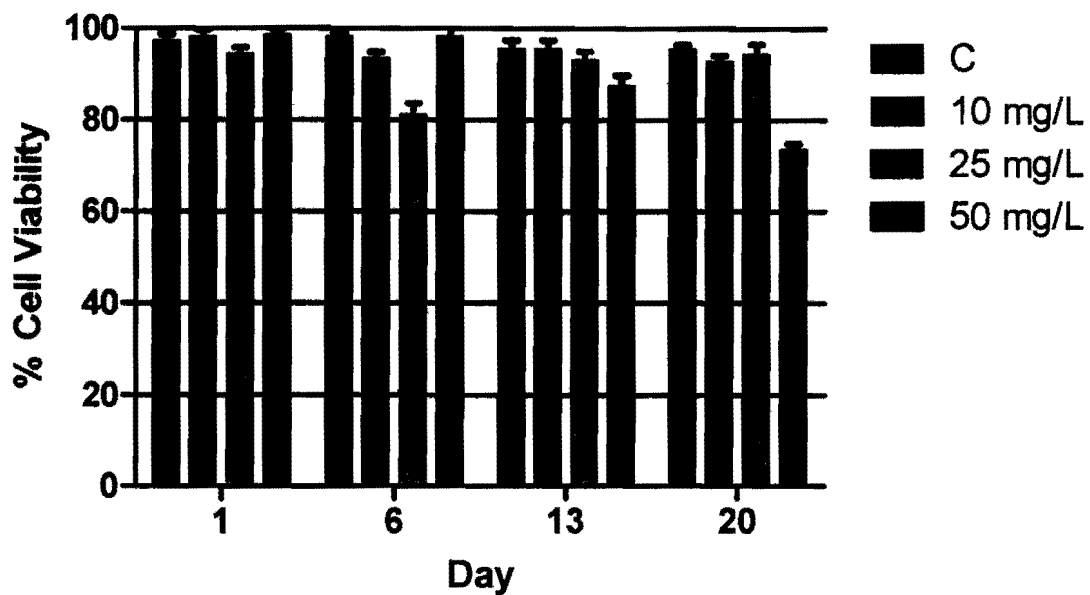


Fig. 4. Cell Viability under Nickel Exposure throughout the Course of the Study. Living cells were considered to have no morphological defects and contained DNA. Dead cells had either a morphology defect or were actually dead and lacked DNA. Percentages of alive cells were calculated and plotted through a 4 week study.

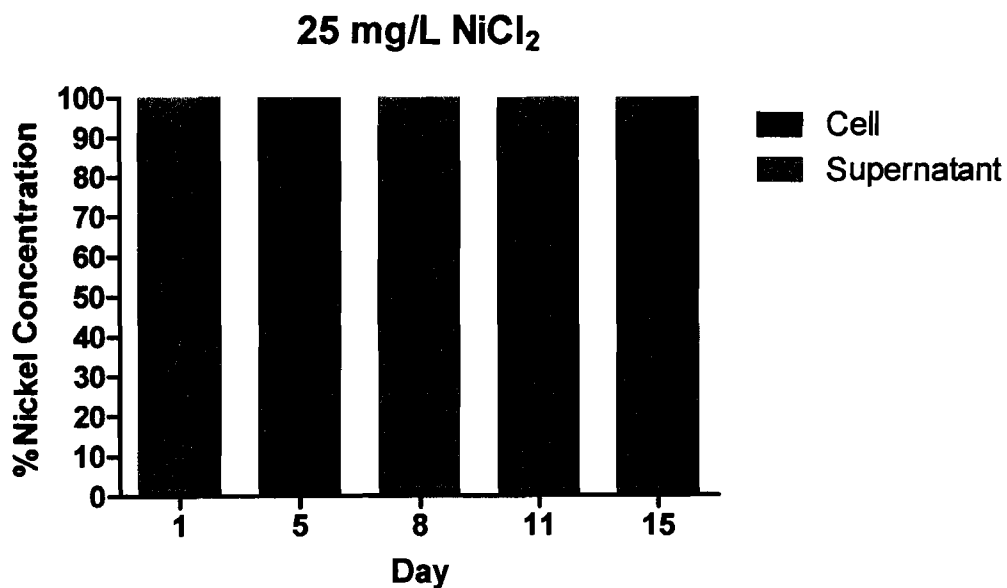
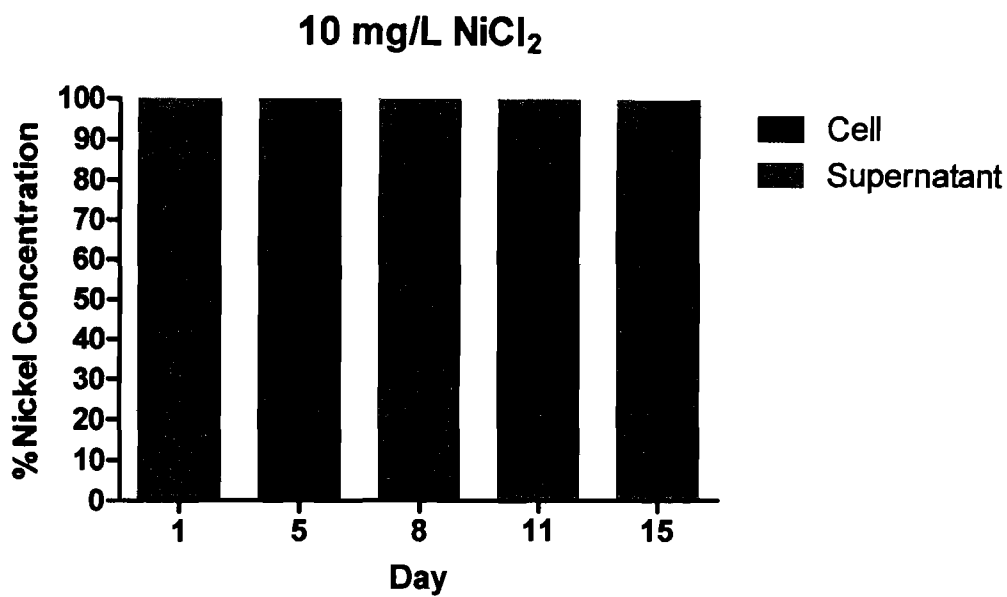


Fig. 5. Distribution of Nickel during the growth of *S. IU 625*. NiCl₂ was initially added to the cells. Nickel dissociates from chloride in an aqueous environment. Raw ICP-MS data was generated examining the nickel concentration against a standard. The raw data was then standardized against the control. The % Nickel Concentration on the y axis represents the increase in nickel over the control.

Metallothionein as a Heavy Metal Response Protein

Metallothionein has been shown to be a heavy metal sequestering protein (Turner 1996). The results of the qPCR data are limited, as only one experiment was performed. Preliminary data indicates that metallothionein may play a role as a nickel response protein in *S. IU 625* (figure 6). The relative quantification data indicates an increase of *smtA* over the housekeeping *rpsL* at day 11 in the culture with 25 mg/L NiCl₂. The 10 mg/L culture remained relatively constant in *smtA* expression levels throughout the study and approximately was always within the standard deviation week to week. The data has been normalized with control and reference samples. Only sample results are shown in the figure 6. The 50 mg/L was not done due to the cell death occurring at such a rapid pace.

The subsequent lower gene expression level of *smtA* in the 10 mg/L compared to control which has no nickel exposure at days 4 and days 11 suggests an alternative mechanism might be at play. Bioinformatic analyses were carried out to better understand the ICP-MS and qPCR results obtained.

Potential Nickel Response Proteins

BlastP results of CnrB and AcrB generated a list of proteins from other strains of *Synechococcus*. The AcrB blast found similarity with *Syn. PCC 7942 HAE1*. HAE1 has been shown to confer a variety of resistances and is a member of the acraflavin family. A multiple sequence alignment with muscle and T-Coffee demonstrated strong homology

with conserved regions. Subsequent neighbor-joining phylogenetic trees were produced with Mega5. The conserved region was visualized with POAVIZ.

Each protein in the survey was approximately 1000 amino acids in length. The conserved region is denoted by the linearity of the sequences in each of the POAVIZ images. The conserved region runs through a significant portion of each protein with some variances in the sequence. This is significant as the phylogenetic tree suggests two different potential functions for the AcrB and CnrB proteins (one being a drug efflux and another being a cation efflux). Multi-drug efflux mechanisms are fairly well established. The strong homology present with the POAVIZ alignment suggests that CnrB might follow a similar mechanism. The variations between CnrB and AcrB are probably due to having a different target substrate for their efflux.

Figure 7 showcases the relationship between genes found in *Syn. PCC 7942* and *Syn. PCC 6301* with known CnrB and other cyanobacteria strains. The localization of *Syn. PCC 7942* and *Syn. PCC 6301* with the multiple sequence alignment suggest CnrB might play a role in cation efflux.

Figure 8 demonstrates a similar relationship with AcrB. AcrB is an efflux protein that has been shown to confer a variety of resistances. The phylogenetic tree demonstrates a strong homology between *Syn. PCC 7942* and *Syn. PCC 6301* across species and suggests a common ancestor. A highly conserved domain was also present.

Figure 9 is a combination phylogenetic analysis of CnrB and AcrB data. The combination tree suggests that each protein confers its own function. The tree is

essentially structured around AcrB and CnrB variants. Subsequent multiple-sequence alignment of all the species' protein demonstrated a strong homology with conserved regions. As the phylogenetic tree suggests a common ancestor might be involved in the development of these two regions of the tree. Ultimately the tree can be divided into two regions based on known function. The AcrB region is potentially a drug resistance branch and the CnrB gene deals with heavy metal or cation efflux. *Syn.* PCC 7942 and *Syn.* PCC 6301 both contain a related family member of each protein in the tree.

S. IU 625 Nickel Response

The expression data of *smtA*, see figure 6, suggests there is an increase in expression levels of 25 mg/L at day 11. The increased expression levels of *smtA* coincide with a decrease in intracellular nickel concentration as seen in the ICP-MS data (figure 5). The 25 mg/L culture at this time was also capable of leaving the extended lag phase and entering the exponential phase as seen in figure 1. *smtA* may have been involved in allowing the cells to start exponential growth at this point. The *smtA* levels coincide with all excess nickel being present in the supernatant at this time. Interesting though, there was no significant up-regulation of *smtA* in the 10 mg/L culture; the levels remained relatively static throughout the study. The *smtA* levels may not have changed drastically in the 10 mg/L culture but the nickel concentration from the ICP-MS data suggests that excess nickel ions were moved into the supernatant, as shown in figure 5. Excess nickel above control was not completely removed until day 11 in the 10 mg/L but this was accomplished a full 3 days earlier in the 25 mg/L at day 8.

The 25 mg/L culture did not fully begin to grow exponentially until after day 11. These observations might mean two potentially different mechanisms are at play. It might be possible that the nickel response mechanism is gauged by cellular sensors and the response is according to the concentration levels (Los 2010). More repeatings are necessary to confirm this trend of gene expression.

The bioinformatic analysis demonstrates a strong homology of a known cation efflux protein, CnrB, with protein from *Syn.* PCC 7942 and *Syn.* PCC 6301. This suggests a potential explanation of the ICP-MS data. The lower expression levels of *smtA* than control for the 10 mg/L culture with nickel still being cleared suggests an alternative mechanism. Efflux proteins present on the membrane can actively pump the heavy metal out. The mechanism is quite similar to that of a multi-drug-efflux protein in which it captures its target, takes it in, and ejects it from the cell. The consensus sequence seen between AcrB and CnrB suggests this mechanism functionality (figure 9). The variation within the consequence sequence could potentially be due to the different substrate binding targets associated with each protein.

Syn. PCC 7942 and *Syn.* PCC 6301 both have family related proteins for AcrB and CnrB within the corresponding phylogenetic trees. Both species contain homologous consequence sequences visualized by POAVIZ, see figures 7, 8. The amino acid length for each protein was approximately 1000. POAVIZ shows a significant portion of the protein length was conserved in *Synechococcus*. A combination of the efflux proteins and SmtA may play a role in nickel resistance.

```

* Block Label: the length of the sequence
SEQ ID 0: gi|428220788|ref|YP_007104958.1 (cation/multidrug [Synechococcus sp. PCC 7502])
SEQ ID 1: gi|170079222|ref|YP_001735860.1 (AcrB/AcrD/AcrF [Synechococcus sp. PCC 7002])
SEQ ID 2: gi|254423090|ref|ZP_05036608.1 (RND, HAE1 [Synechococcus sp. PCC 7335])
SEQ ID 3: gi|56751744|ref|YP_172445.1 (RND multidrug [Synechococcus elongatus PCC 6301])
SEQ ID 4: gi|113011781|ref|YP_41305.1 (HAE1 [Synechococcus elongatus PCC 6301])
SEQ ID 5: gi|113011781|ref|YP_41305.1 (HAE1 [Synechococcus elongatus PCC 6301])
SEQ ID 6: gi|116074385|ref|ZP_01471647.1 (RND multidrug efflux [Synechococcus sp. RS9916])
SEQ ID 7: gi|352096483|ref|ZP_08957310.1 (acriflavin resist [Synechococcus sp. MH 8016])
SEQ ID 8: gi|87125001|ref|ZP_01060848.1 (RND multidrug efflux [Synechococcus sp. RS9917])
SEQ ID 9: gi|113954483|ref|YP_729337.1 (acriflavin resist acrF [Synechococcus sp. CC9311])
SEQ ID 10: gi|113954483|ref|YP_729337.1 (acriflavin resist acrF [Synechococcus sp. CC9311])
SEQ ID 11: gi|352096483|ref|ZP_08957310.1 (acriflavin resist [Synechococcus sp. MH 8016])
SEQ ID 12: gi|352096483|ref|ZP_08957310.1 (acriflavin resist [Synechococcus sp. MH 8016])

```

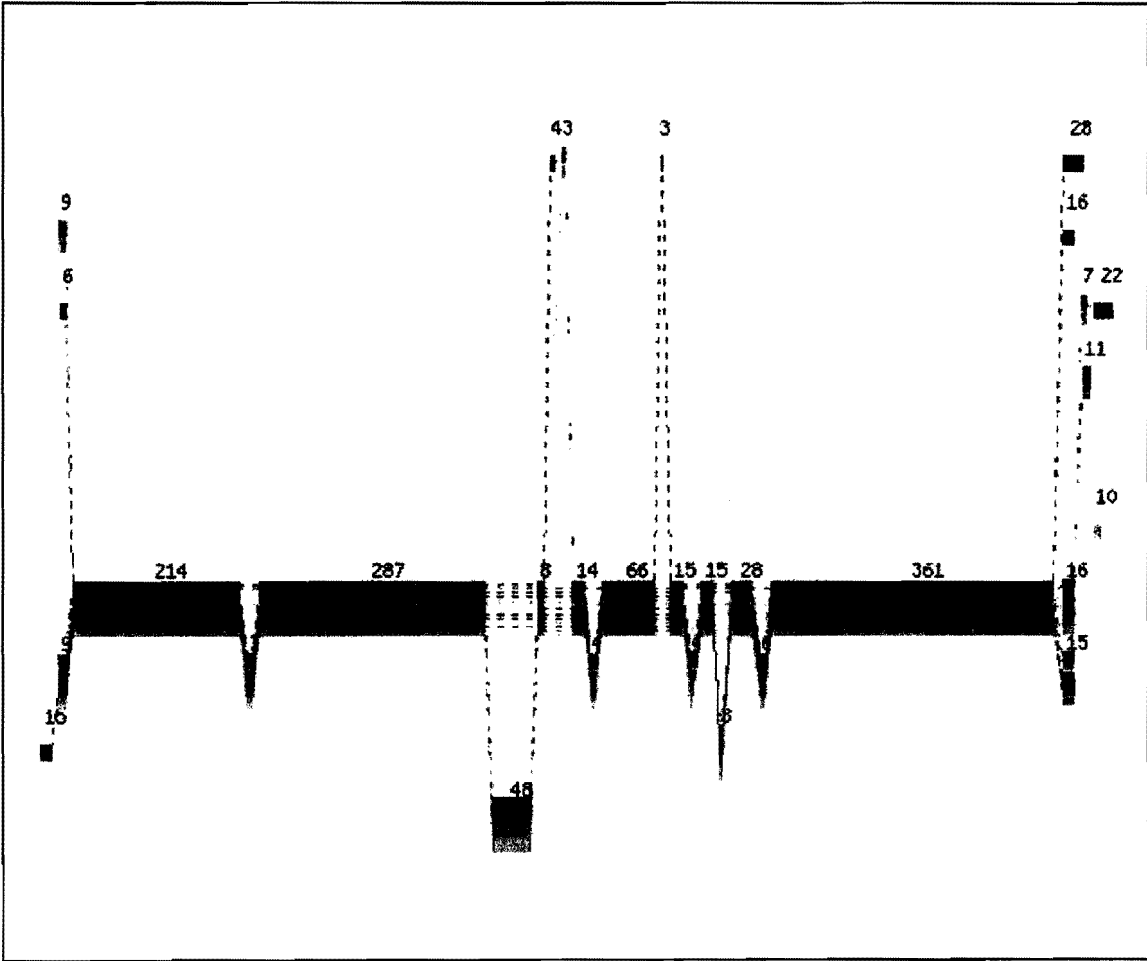


Fig. 8a. Partial Order Alignment of AcrB. POA VIZ was used to visualize the multiple sequence alignment results. There is strong homology amongst the 13 species surveyed, with 3-4 conserved regions.

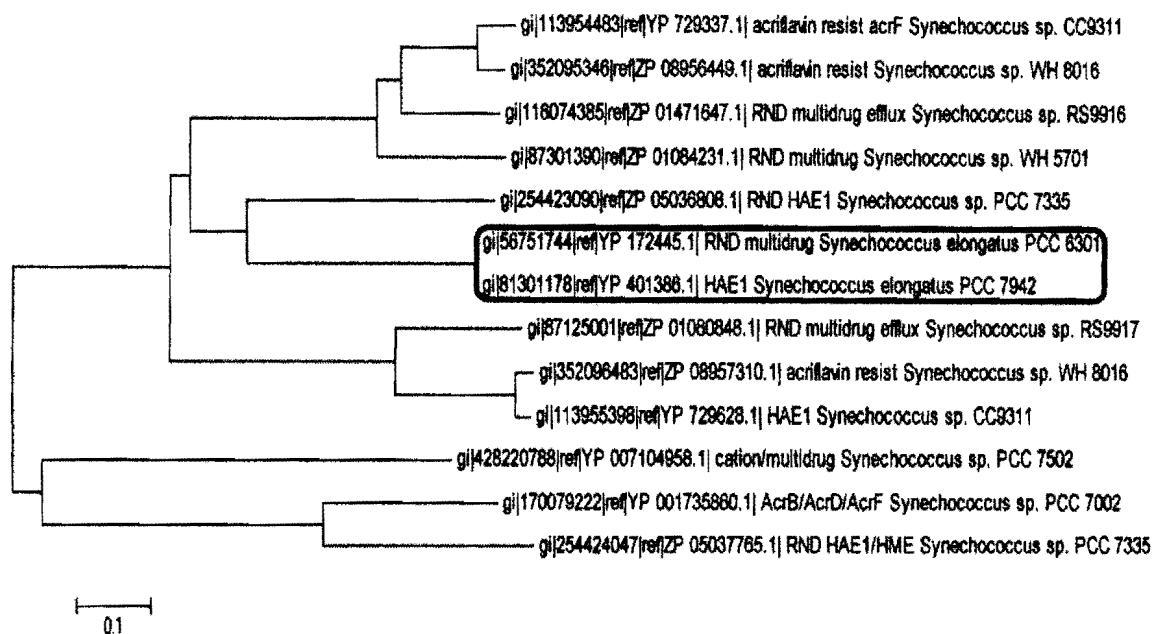


Fig. 8b. Phylogenetic Tree of a known transport protein, AcrB. 13 species of cyanobacteria were chosen via BlastP with AcrB. Multiple-Sequence-Alignment was done with Muscle in Mega5. A neighbor-joining phylogenetic tree was generated from this data. *Syn.* PCC 7942 and *Syn.* PCC 6301 (highlighted) both have high homology and are located within the multidrug resistance bifurcation clade.

SEQ ID 0: gi|428220788|ref|YP_007104958.1 (cation/multidrug [Synechococcus sp. PCC 7502])
 SEQ ID 1: gi|170079222|ref|YP_001735860.1 (AcrB/AcrD/AcrF [Synechococcus sp. PCC 7002])
 SEQ ID 3: gi|56751744|ref|YP_172445.1 (RND multidrug [Synechococcus elongatus PCC 6301])
 SEQ ID 4: gi|81301178|ref|YP_401386.1 (HAE1 [Synechococcus elongatus PCC 7942])
 SEQ ID 22: gi|81301178|ref|YP_401386.1 (HAE1 [Synechococcus elongatus PCC 7942])
 SEQ ID 23: gi|56751744|ref|YP_172445.1 (RND multidrug [Synechococcus elongatus PCC 6301])
 SEQ ID 7: gi|352096483|ref|ZP_08957310.1 (acriflavin resist [Synechococcus sp. WH 8016])
 SEQ ID 10: gi|113955398|ref|YP_729628.1 (HAE1 [Synechococcus sp. CC9311])
 SEQ ID 27: gi|113955398|ref|YP_729628.1 (transporter HAE1 [Synechococcus sp. CC9311])
 SEQ ID 25: gi|260435885|ref|ZP_05789855.1 (multidrug,Hydrophobe Synechococcus sp. WH 8109)
 SEQ ID 8: gi|87125001|ref|ZP_01080848.1 (RND multidrug efflux [Synechococcus sp. RS9917])
 SEQ ID 13: gi|428221553|ref|YP_007105723.1 (HM efflux pump [Synechococcus sp. PCC 7502])
 SEQ ID 15: gi|352094055|ref|ZP_08955226.1 (HM efflux pump, CzcA [Synechococcus sp. WH 8016])
 SEQ ID 16: gi|352094055|ref|ZP_08955226.1 (HM efflux pump, CzcA [Synechococcus sp. WH 8016])
 SEQ ID 17: gi|113952990|ref|YP_730715.1 (cation efflux czcA-1 [Synechococcus sp. CC9311])
 SEQ ID 19: gi|148242812|ref|YP_001227969.1 (cation efflux [Synechococcus sp. RCC307])
 SEQ ID 18: gi|88808347|ref|ZP_01123857.1 (cation / drug efflux [Synechococcus sp. WH 7805])
 SEQ ID 14: gi|427713784|ref|YP_007062408.1 (HM efflux pump [Synechococcus sp. PCC 6312])
 SEQ ID 28: CONSENSO (consensus produced by heaviest_bundle, containing 0 seqs)
 SEQ ID 21: gi|427714346|ref|YP_007062970.1 (cation/multidrug [Synechococcus sp. PCC 6312])
 SEQ ID 6: gi|116074385|ref|ZP_01471647.1 (RND multidrug efflux [Synechococcus sp. RS9916])
 SEQ ID 9: gi|56751744|ref|YP_172445.1 (RND multidrug [Synechococcus elongatus PCC 6301])
 SEQ ID 11: gi|352095346|ref|ZP_08956449.1 (acriflavin resist [Synechococcus sp. WH 8016])
 SEQ ID 24: gi|352095346|ref|ZP_08956449.1 (acriflavin resist [Synechococcus sp. WH 8016])
 SEQ ID 12: gi|87301390|ref|ZP_01084231.1 (RND multidrug [Synechococcus sp. WH 5701])
 SEQ ID 5: gi|254424047|ref|ZP_05037765.1 (RND, HAE1/HME [Synechococcus sp. PCC 7335])
 SEQ ID 20: gi|254424047|ref|ZP_05037765.1 (RND, HAE1/HME family [Synechococcus sp. PCC 7335])
 SEQ ID 2: gi|254423090|ref|ZP_05036800.1 (RND, HAE1 [Synechococcus sp. PCC 7335])
 SEQ ID 26: gi|56751744|ref|YP_172445.1 (RND multidrug [Synechococcus elongatus PCC 6301])

Fig. 9a. Synechococcus Species used for POA Analysis. List of species and corresponding protein, CnrB and AcrB used in partial order alignment for combination.

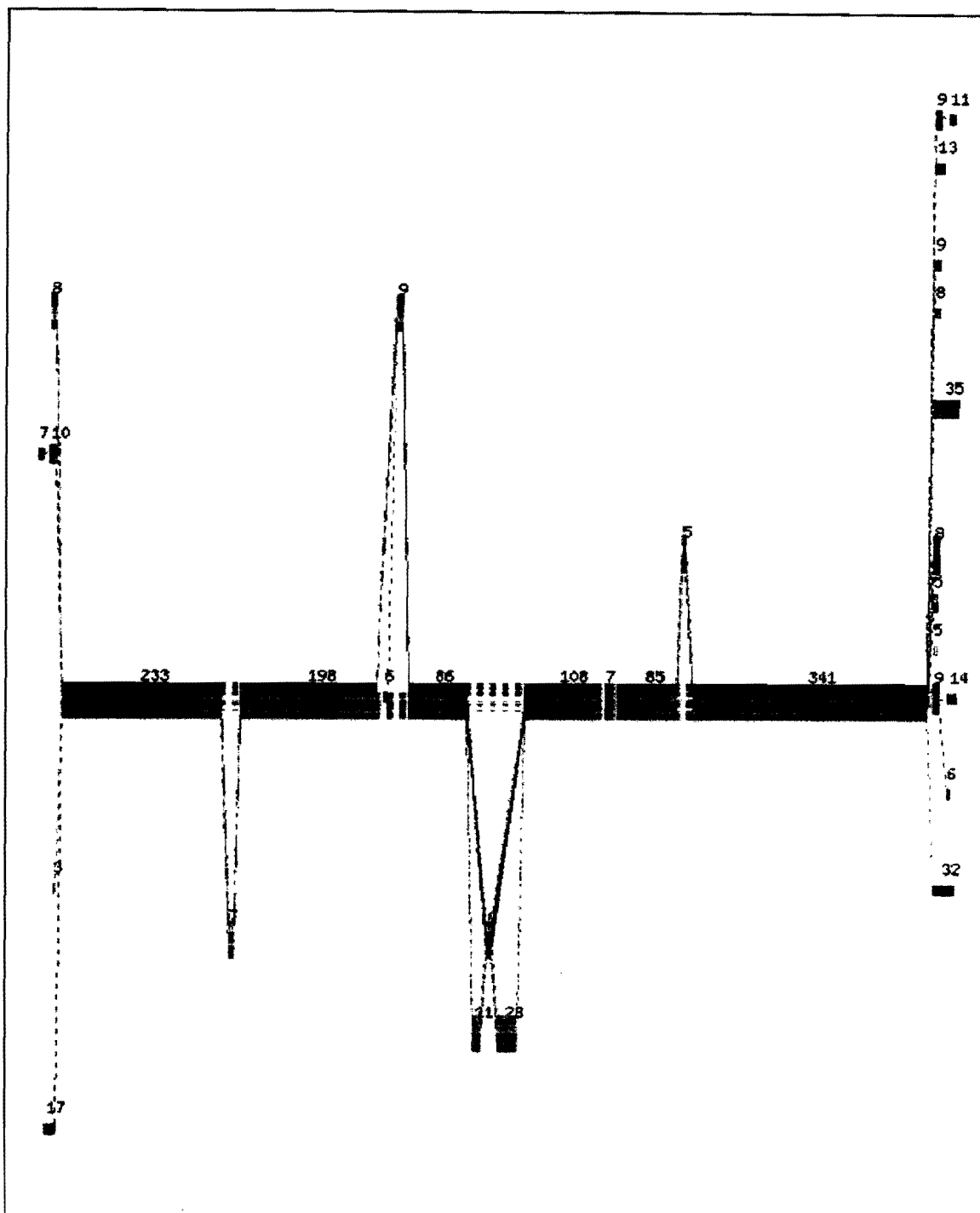


Fig. 9b. Partial Order Alignment of CnrB and AcrB. Both sets of proteins were aligned, this dataset contained 26 species. The image highlights a consequence sequence, visualized by POAVIZ. The linearity of the sequence demonstrates high homology between two different proteins across species surveyed.

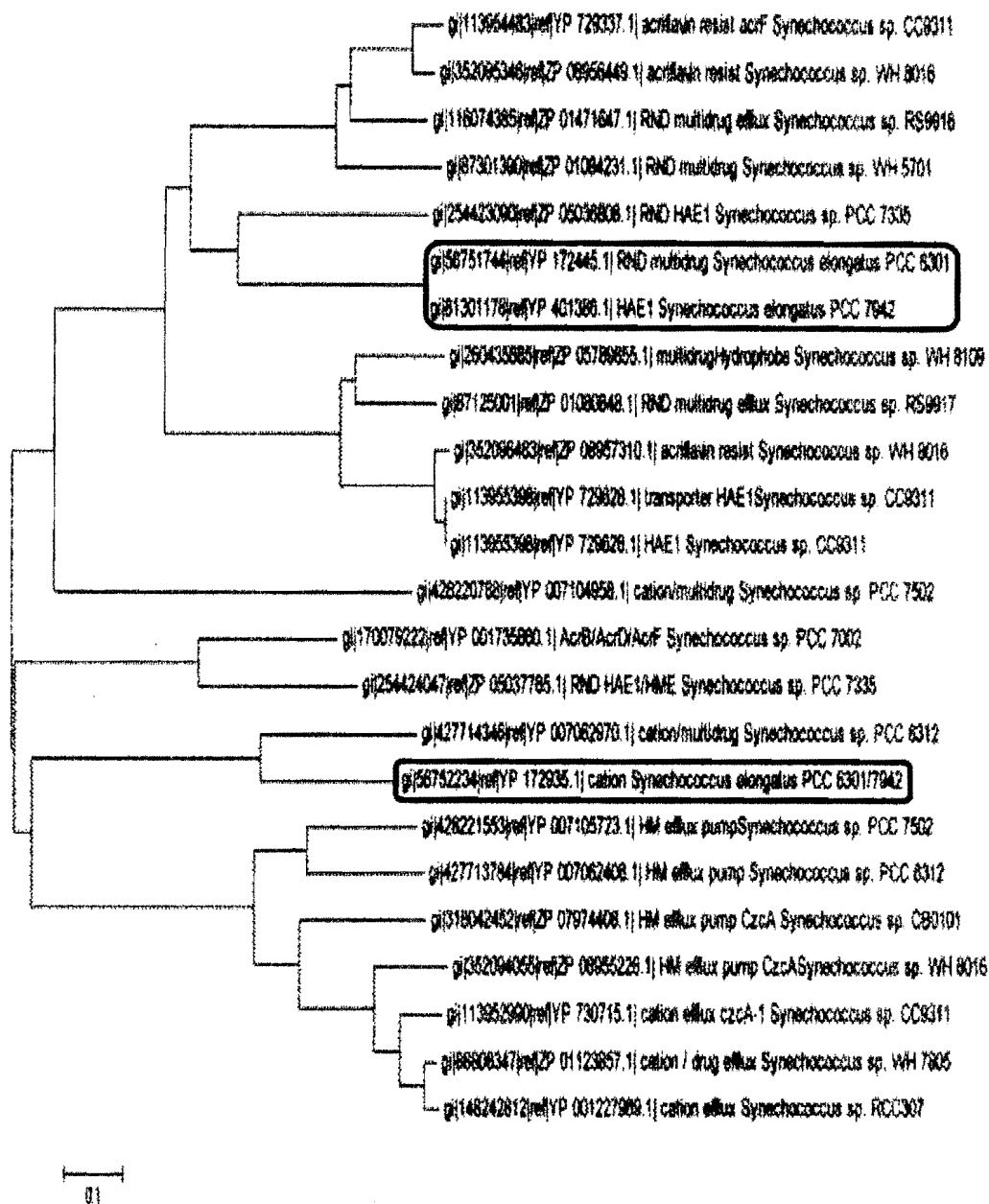


Fig. 9c. Phylogenetic Analysis of CnrB and AcrB. Both sets of CnrB and AcrB data were combined and aligned via Muscle in Mega5. Two different proteins of interest are found in *Syn.* PCC 7942 and *Syn.* PCC 6301. The tree is bifurcated with function being either drug resistance or heavy metal resistance. *Syn.* PCC 7942 and *Syn.* PCC 6301 each have a protein embedded within the branch suggesting function. Both proteins have high homology in their sequence.

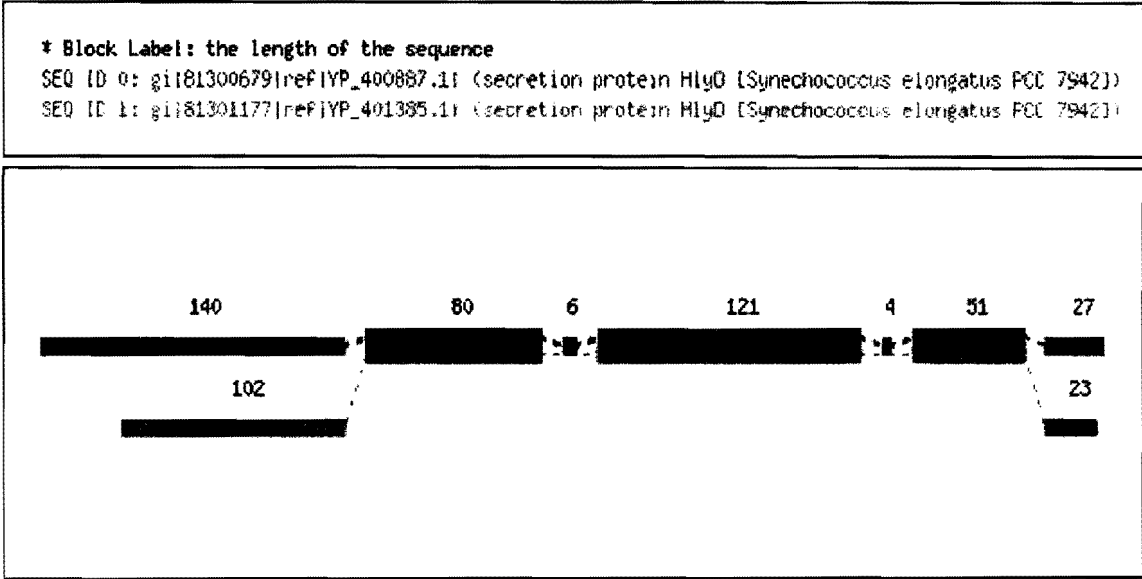


Fig. 10. Partial Order Alignment of hylD. *hylD* is located upstream of both *Syn.* PCC 7942 genes, it is a secretion protein involved in both heavy metal efflux and multi-drug efflux operons.

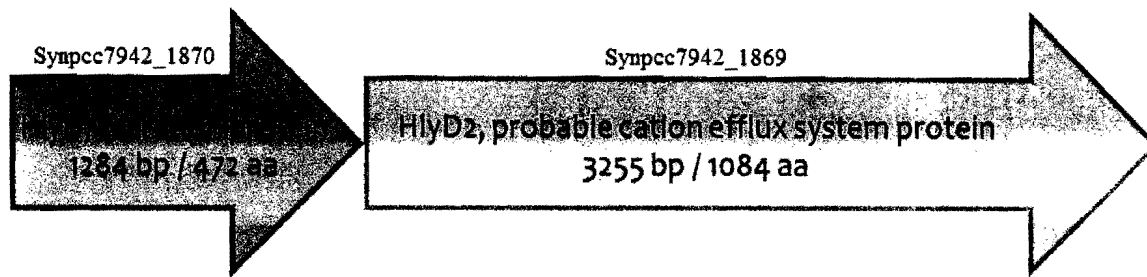


Fig. 11. Potential *nsr* Operon. *hylD* is located upstream of *nsrB/hlyD2*. *hylD* is often associated with efflux genes.

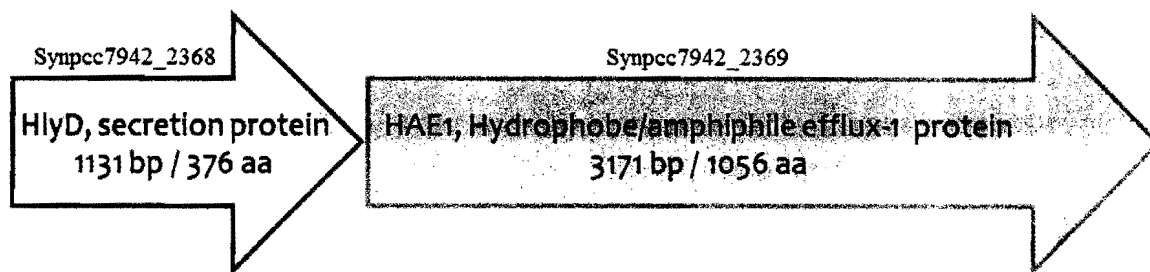


Fig. 12. Potential *hae* Operon. *hylD* is often found upstream of efflux genes. *hylD* is gene Synpcc7942_2368 in the above image, the *HAE1* gene is Synpp7942_2369. The association of *hylD* with an efflux gene constitutes a typical promoter.

Conclusions and Discussion

S. IU 625 demonstrates a remarkable ability to adapt and grow in high nickel concentration conditions. Nickel is normally at “trace” levels in the environment, 0.3 ppb in rivers (Wright 2003). The experiment present here assesses growth that is well above what cells would normally be exposed to. The cells were capable of growing in 10 mg/L and exhibited delayed growth in 25 mg/L. The 50 mg/L was too high a concentration and lead to no growth and eventual death of the culture. Cells at higher concentration of nickel initially accumulated defects at a higher rate. The defects include changes in morphology such as a vibrio-shape, altered cell-size, and fragmented DNA (figure 3). The most notable defect was a bleaching of the cells in the 25 mg/L culture. Bleaching involves a change or loss of coloration in the cells. Figure 2 shows overtime the 25 mg/L culture became a pale green as opposed to a darker green in the control. Interestingly, the corresponding cell number, see figure 1, increased during this timeframe. Together, this suggests potential damage to the pigments normally found in the cyanobacteria. The 25 mg/L culture was capable of fixing the damage and finished the study with a similar dark green coloration to that of the control.

An increase in cell death was also present with higher nickel concentrations. The 50 mg/L had virtually no growth throughout the study. The 10 mg/L had an initial increase in dead cells but returned to levels appreciable to that of 0 mg/L. At day 5 the cell numbers were within a standard deviation between the control and 10 mg/L cultures, both cultures grew increasingly closer in cell number as the study continued on, see figure 1. The 25 mg/L had a drastic increase in dead cells within the first week but by the

end of the second week returned to levels similar to 0 mg/L. The 25 mg/L demonstrated a prolonged lag phase up to day 11 with rapid growth following. The cells also returned to a healthy green color similar to that of the control at this time, see figure 2. The cells were capable of overcoming significant defects to their pigmentation and grew at a rapid rate initially after. Further data provides some insight into understanding this drastic response.

The cell membrane is selectively permeable which allows ions and molecules to cross in and out of the cell. Molecules can be actively transported across the membrane or diffusion can occur through ion channels if a concentration gradient is present. The permeability of the membrane plays an important role in the way nickel crosses the membrane in *S. IU 625* and the cell's response. The ICP-MS data provides an understanding of this process.

The raw data from ICP-MS was standardized against the control levels. Therefore the data present in figure 5 is the % of nickel concentration increase over the control. Cells initially became flushed with nickel. The 10 mg/L culture and 25 mg/L had similar increases in nickel concentration at day 5. Interestingly, this also coincides with the time the 10 mg/L culture was able to leave the extended lag phase and continue growing, see figure 1. At day 8, nickel concentration in the 10 mg/L culture remained higher than the 25 mg/L. The 10 mg/L culture continued to grow despite having elevated nickel levels. By day 11 nickel concentrations within both cultures were similar to that of the 0 mg/L. The 10 mg/L culture had no difference to the 0 mg/L culture and the 25

mg/L had an increase of only 1% nickel. The timeframe between days 11-13 in the 25 mg/L culture seems to be a critical time-point for cellular recovery. The population became stabilized with a reduction in dead cells and an increase in living cells. The 25 mg/L culture began to grow rapidly at day 11, see figure 1, this coincides with the removal of the excess nickel at this time. Cellular pigmentation was recovered around this time in the 25 mg/L culture, see figure 2.

The survival mechanisms for cell survival in this harsh environment kept excess nickel essentially out of the cell. Based on the ICP-MS data only the 50 mg/L culture was overwhelmed with nickel and could not effectively keep the nickel concentration at a survivable level. The 25 mg/L culture did retain some excess nickel throughout the study but that did not impact cell growth after day 11 see figure 1, since the cells grew rapidly after.

The mechanism(s) describing the way *S. IU 625* survives in the increased nickel concentration remains unclear. Noted earlier, cell aggregation was demonstrated in the 25 mg/L culture but not in the 50 mg/L culture. Cell aggregation could potentially minimize exposure to the environment and may play a role in nickel defense. The same 25 mg/L culture that demonstrated cell aggregation on day 13 did not show as a pronounced cell aggregation by day 20. Cell aggregation may slow the intake of nickel. But the ICP-MS data suggests that nickel is still being actively removed from the cells in some way.

Metallothionein is a known heavy metal sequester protein, primarily used for zinc, cobalt, and cadmium defense (Chu 2012). The qPCR data is preliminary and the data is inconclusive. Metallothionein may play a minimal role in nickel response as a long-term defense mechanism. In eukaryotic mice models, metallothionein over-expression did not confer any resistance to nickel-related damage (Wallkes 2004). The qPCR data only examines the response 72+ hours after nickel exposure. The mechanism of metallothionein is that the repressor is removed during high concentrations of heavy metal, primarily zinc.

The proteins and there corresponding genes identified through bioinformatics need to be investigated fully using PCR identification and knock-out studies. Further *smtA* analysis is needed through repeating of long-term studies to clarify the results of the expression levels. Short terms studies, those in which cells have been exposed less than 24 hours, need to be done as well. Analysis short-term study data for ICP-MS and *smtA* will provide a fuller picture of the cellular stress response.

The nickel response mechanism by *S. IU 625* might be multi-faceted encompassing many different proteins at various stages through exposure. Metallothionein may act as a short term response element until the larger, more energy costly, cation efflux proteins are translated and embedded within the membrane. A genomic analysis looking at different genes being active at different times in the study will provide the clearest indication of *S. IU 625* heavy metal response.

More data is necessary to generate any conclusions regarding nickel accumulating on the cell surface and cell aggregation. The mechanism behind the bleaching effect also remains unknown. It is suggested that this effect might be due to pigmentation damaged caused by nickel. But it remains untested experimentally.

More research is needed in this area since pollution is a real world concern that continues to be an increasing problem world-wide. Cyanobacteria have shown there capacity to grow in harmful environments. These strains of bacteria are also capable of leaving behind toxins which can be detrimental to human health. But this is a unique opportunity to study there defense mechanisms and use inactivated forms to fix polluted areas.

Works Cited

- Azeez, P. A. and D. K. Banerjee. "Nickel uptake and toxicity in cyanobacteria." *Toxicological and Environmental Chemistry* (1991): 43-50.
- Banak, Sandra A., Tracie Al. Caller and Elijah W. Stommel. "The Cyanobacteria Derived Toxin Beta-N-Methylamino-L-Alanine and Amyotrophic Lateral Schlerosis." *Toxins* (2010): 2837-2850.
- Boisvert, Steve, et al. "Inhibition of the Oxygen-evolving Complex of Photosystem II and Depletion of Extrinsic Polypeptides by Nickel." *BioMetals* (2007): 879-889.
- Brand, Larry E., et al. "Cyanobacterial Blooms and the Occurance of the neurotoxin beta-N-methylamino-L-alanine (BMAA) in South Florida Aquatic Food Webs." *Harmful Algae* (2010): 620-635.
- Caballero, Hermes Reyes, Gregory C. Campanello and David P. Giedroc. "Metalloregulatory Proteins: Metal Selectivity and Allosteric Switching." *Biophys Chem* (2011): 103-114.
- Cavet, Jennifer S., et al. "A Nickel-Cobalt-sensing ArsR-SmtB Family Repressor." *The Journal of Biological Chemistry* (2002): 38441-38448.
- Chakraborty, Parthasarathi , et al. "Stress and toxicity of biologically important transition metals (Co, Ni, Cu and Zn) on phytoplankton in a tropical freshwater system: An investigation with pigment analysis by HPLC." *Chemosphere* (2010): 548-553.
- Chu, T. C., et al. "Adaptations of *Synechococcus* sp. IU 625 to Growth in the Prescence of Mercuric Chloride." *Acta Histochemica* (2012): 6-11.
- Chu, T.-C., et al. "Identification of *Synechococcus* sp. IU 625 metallothionein gene and its evolutionary relationship to the metallothionein gene of other cyanobacteria." *The 2007 International Conference on Bioinformatics & Computational Biology (BIOCOMP 2007)* (2007): 201-207.
- Danilov, Roman A. and Nils G.A. Ekelund. "Effects of Cu²⁺, Ni²⁺, Pb²⁺, Zn²⁺ and pentachlorophenol on photosynthesis and motility in *Chlamydomonas reinhardtii* in short term exposure experiments." *BMC Ecology* (2001): 1:1.
- Ettinger, Thomas, et al. "Secondary transporters for nickel and cobalt ions: Theme and variations." *BioMetals* (2005): 399-405.

- Foster, Andrew W., et al. "Cytosolic Ni(II) Sensor in Cyanobacterium." *Journal of Biological Chemistry* (2012): 12142-12151.
- Franke, Sylvia, et al. "Molecular Analysis of the Copper-Transporting Efflux System CuSCFBA of *Escherichia coli*." *Journal of Bacteriology* (2003): 3804-3812.
- Garcia-Dominguez, Mario and et al. "A Gene Cluster Involved in Metal Homeostasis in the Cyanobacterium *Synechocystis* sp. Strain PCC 6803." *Journal of Bacteriology* (2000): 1507-1514.
- Gardea-Torresdey, J. L., et al. "Ability of Immobilized cyanobacteria to remove metal ions from solution and demonstration of the presence of metallothionein genes in various strains." *Journal of Hazardous Substance Research* (1998): 2:1-18.
- Hemlata, Tasneem Fatma. "Screening of Cyanobacteria for Phycobiliproteins and Effect of Different Environmental Stress on Its Yield." *Bull Environ Contam Toxicol* (2009): 509-515.
- Lawrence, J. R., et al. "Microscale and Molecular Assessment of Impacts of Nutrients and Oxygen Level on Structure and Function of River Biofilm Communities." *Applied and Environmental Microbiology* (2004): 4326-4339.
- Lee, L. H. and B. Lustigman. "Effect of Barium and Nickel on Growth of *Anacystis nidulans*." *Environmental Contamination and Toxicology* (1996): 985-992.
- Los, Dmitry A., et al. "Stress Sensors and Signal Transducers in Cyanobacteria." *Sensors* (2010): 2386-2415.
- Lustigman, B., L. H. Lee and A. Khalil. "Effects of Nickel and pH on the Growth of *Chlorella vulgaris*." *Environmental Contamination and Toxicology* (1995): 73-80.
- Mishra, Shruti and R. S. Dubey. "Heavy Metal Toxicity Induced Alterations in Photosynthetic Metabolism in Plants." Pessarakli, M. *Handbook of Photosynthesis*. Taylor & Francis Group LLC, 2005. 845-864.
- Perrin, Claire, et al. "Nickel Promotes Biofilm Formation by *Escherichia coli* K-12 Strains That Produce Curli." *Applied and Environmental Microbiology* (2009): 1723-1733.
- Rodionov, Dmitry A., et al. "Comparative and Functional Genomic Analysis of Prokaryote Nickel and Cobalt Uptake Transporters: Evidence for a Novel Group of ATP-Binding Cassette Transporters." *Journal of Bacteriology* (2006): 317-327.

- Schor-Fumbarov, Tamar and Peter B. Goldsbrough. "Characterization and expression of a metallothionein gene in the aquatic fern *Azolla filiculoides* under heavy metal stress." *Planta* (2005): 69-76.
- Tchou-Wong, Kam Meng, et al. "Effects of Nickel Treatment on H3K4 Trimethylation and Gene Expression." *PLoS ONE* (2011): 1-10.
- Tian, Jian, Wu, Ningfeng Li, Jian, et al. "Nickel-Resistant Determinant from *Leptospirillum ferriphilum*." *Applied and Environmental Microbiology* (2007): 2364-2368.
- Turner, Jennifer S. "Zn²⁺-sensing by the cyanobacterial metallothionein repressor SmtB: different motifs mediate metal-induced protein-DNA dissociation." *Nucleic Acids Research* (1996): 3714-3721.
- Velikova, Violeta and Tsonko Tsonev. "Changes in photosynthesis, mesophyll conductance to CO₂, and isoprenoid emissions in *Populus nigra* plants exposed to excess nickel." *Environmental Pollution* (2011): 1058-1066.
- Wallkes, Michael P., et al. "Minimal influence of metallothionein over-expression on nickel carcinogenesis in mice." *Toxicology Letters* (2004): 357-364.
- Wang, Bin, et al. "Effects of Cd, Cu, Ni, and Zn on Brown Tide Alga *Aureococcus Anophagefferens* Growth and Metal Accumulation." *Environmental Science and Technology* (2012): 517-524.
- Wright, John. "Heavy metals and pollution of the lithosphere." Wright, John. *Environmental Chemistry*. London: Routledge, 2003. 198-224.
- Zhang, Yan, et al. "Comparative genomic analyses of nickel, cobalt and vitamin B12 utilization." *BMC Genomics* (2009).
- Zhou, Xue, et al. "Effects of Nickel, Chromate, and Arsenate on Histone 3 Lysine Methylation." *Toxicology Applied Pharmacology* (2009): 78-84.

**THE EFFECTS OF NICKEL CHLORIDE STRESS ON FRESHWATER
CYANOBACTERIUM *SYNECHOCOCCUS* SP. IU 625**

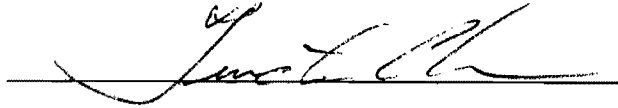
BY

BRIAN NOHOMOVICH

Submitted in partial fulfillment of the requirements for the
degree of Master of Science in Biology from the
Department of Biological Sciences of Seton Hall University

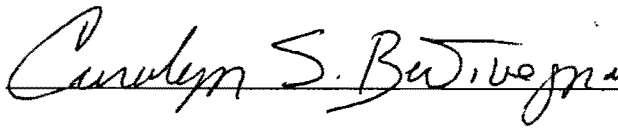
May 2013

APPROVED BY



MENTOR

Dr. Tin-Chun Chu



COMMITTEE MEMBER

Dr. Carolyn Bentivegna



COMMITTEE MEMBER

Dr. David Sabatino



DIRECTOR OF GRADUATE STUDIES

Dr. Allan Blake



CHAIR, DEPARTMENT OF BIOLOGICAL SCIENCES

Dr. Jane Ko

Acknowledgment

Dr. Chu, thank you for all the advice, support, and for providing much needed assistance through our busy schedules.

To my committee, I would like to thank you for reviewing this work and providing much needed feedback.

I am very grateful to Michael Quintanilla and Naturex for performing the ICP-MS work. Your hard work provided a key part of this data.

Finally I extend gratitude to Robert Newby for helping me when I needed it, the Biology Department, and Seton Hall University for making this project possible.

Table of Contents

Introduction	1
Materials and Methods	4
Results	9
Conclusion & Discussion	34
Work Cited	39

List of Figures

Figure 1	Growth Curves of <i>S. IU 625</i> with or without Nickel Stress	13
Figure 2	Pigment Visualization	14
Figure 3	Microscopic Observations of <i>S. IU 625</i> with Various Nickel Concentrations at Day 13	15
Figure 4	Cell Viability under Nickel Exposure throughout the Course of the Study	16
Figure 5	Distribution of Nickel during the growth of <i>S. IU 625</i>	17
Figure 6	Relative Quantification of <i>smtA</i>	23
Figure 7a	Partial Order Alignment (POA) of CnrB	24
Figure 7b	Phylogenetic Analysis of CnrB in <i>Synechococcus</i>	25
Figure 8a	Partial Order Alignment (POA) of AcrB	26
Figure 8b	Phylogenetic Analysis of AcrB in <i>Synechococcus</i>	27
Figure 9a	<i>Synechococcus</i> Species used for POA Analysis	28
Figure 9b	Partial Order Alignment (POA) of CnrB and AcrB	29
Figure 9c	Phylogenetic Analysis of CnrB and AcrB	30
Figure 10	Partial order Alignment (POA) of <i>hlyD</i>	31
Figure 11	Potential <i>nsr</i> Operon	32
Figure 12	Potential <i>hae</i> Operon	33

Abstract

The ability of cyanobacteria to grow in heavy metal polluted areas is proving a challenge to environmental restoration initiatives. Cyanobacteria secrete toxins, such as microcystins that are potentially dangerous to human health. Thus, it is an imperative to investigate the cyanobacteria response against heavy metals to gain insight into their remarkable stress response. Understanding this stress response may someday provide insight into combating the algal blooms formed from high densities of cyanobacteria or perhaps means to cure heavy metal polluted areas. By understanding the way cyanobacteria can thrive in these environments, strategies can be developed to counteract them.

To further develop an understanding of the stress response, the physiology of cyanobacteria was assessed to nickel exposure. Cultures were grown in increasing concentrations of nickel chloride. Cell morphology was assessed through microscopy. Cell counts and turbidity provided insight into cell growth. ICP-MS examined the movement of nickel ions within the cell to the outside of the cell through the course of the environment. qPCR of a known heavy metal response gene, *smtA*, provides analysis of potential response mechanism. Finally, bioinformatic analyses provide an understanding of the observed ICP-MS data by highlighting potential nickel response proteins based on homology and phylogeny, as well as the possible resistance mechanism of nickel stress in freshwater cyanobacteria.

Introduction

The formation of algal blooms is a serious concern worldwide for human and animal health. Algal blooms cause oxygen depletion in the aquatic environment. Algal blooms form from the increase use of pesticides, fertilizer, and waste (Brand 2010). The nutrient-enriched environments cause a dramatic increase in the cyanobacteria population and a subsequent decrease in other competing bacteria. The cyanobacteria will then become the dominant population in the aquatic environment. Many species of cyanobacteria secrete toxic metabolites (Banack 2010, Brand 2010). For example, the toxin Beta-N-Methylamino-L-Alanine (BMAA) has been linked to various diseases and is considered a factor in Alzheimer's disease (Banack 2010). Monitoring of global water bodies has become a human health imperative. The way cyanobacteria manage to thrive in heavy metal polluted environments needs to be further evaluated.

The freshwater bacterium, *Synechococcus* sp. IU 625 (*S. IU 625*) is a unicellular rod-shaped microorganism with a similar cell wall structure to Gram-negative bacteria (Chu 2012). *S. IU 625* is an ideal candidate to study heavy metal response mechanisms due to its fast growth, easy maintenance/cultural conditions, and strong homology with two fully sequenced genomes, *Synechococcus elongatus* PCC 7942 (*Syn. PCC 7942*) and *Synechococcus elongatus* PCC 6301 (*Syn. PCC 6301*) (Chu 2012). The unique nature of cyanobacteria to grow in a wide range of environmental conditions makes it an ideal model. Using *S. IU 625* as a model, many biological processes can be assessed including cell cycle, membrane transport and various molecular mechanisms. The use of genome amplification allows for a way to monitor cellular response to a heavy metal stress.

Metallothionein (MT) is a heavy metal stress response protein. *smtA* is the gene that encodes MT. The gene *smtB* encodes a repressor that blocks the transcription of *smtA* (Chu 2007). Binding of heavy metal ions to the repressor exposes the *smtA* binding site allowing for transcription to proceed (Turner 1996). Metallothionein sequesters free heavy metal divalent cations. MT will then be expelled from the cell containing the heavy metals. It has been previously demonstrated that increase expression of MT can increase cell survival in a heavy metal stress environment. Metallothionein has been shown to confer an increased resistance to cadmium, zinc, mercury, and copper (Chu 2007). Previous studies have shown that increasing concentrations of heavy metals can slow cell growth (Lee 1996). Expanding on the previous work, nickel was chosen as a heavy metal stress.

Nickel is an essential metal that plays an important role in health of eukaryotes and prokaryotes (Rodionov 2006). Nickel is a necessary cofactor for enzymatic function in prokaryotes (Rodionov 2006, Zhang 2009). Nickel-associated enzymes play a crucial role in maintaining the global cycle for nitrogen, carbon, and oxygen (Zhang 2009). However, high concentrations of nickel exposure could be potentially toxic. Nickel has been shown to cause detrimental damage to lung tissue (Tchou-Wong 2011, Zhou 2009) and is categorized as a potential carcinogen (Tchou-Wong 2011). It is also a target analyte for the Environmental Protection Agency (EPA). In human cell lines, nickel accumulates intracellularly and effects DNA methylation and iron-uptake systems resulting in iron deficiency. Nickel can impair gene expression levels through an

epigenetic mechanism by increasing the number of DNA methylations present on promoter regions (Tcho-Wong 2011, Zhou 2009).

Cyanobacteria and other prokaryotes can directly be damaged by nickel as well. Nickel can target or interfere with important enzymes involved in photosynthesis (Boisvert 2007, Hemlata 2009). The mechanism of this damage is still undefined but it is thought that nickel acts as free-radical initiator which induces severe damage to the photosystem (Boisvert 2007). Nickel can also bind to the cell wall of the bacteria inducing stress (Lee 1996). Binding of nickel to the cell wall is a biosorption mechanism which has been proposed as a means to clean polluted areas (Gardea-Torresdey 1998, Azeez 1991). The damaging effects of nickel have allowed prokaryotes to develop a wide range of survival methods.

The primary methods in which prokaryotes combat stress are through an efflux protein (Ettinger 2005), a sequestering metal chelate such as metallothionein (Garcia-Domingues 2000, Turner 1996), formation of biofilms as seen in *E. coli* (Perrin 2009) or to turn the harmful heavy metal ion into a neutral molecule. Previous work has shown that *S. IU 625* sequesters or utilizes an efflux mechanism to maintain homeostasis of heavy metal (Chu 2012, Lee 1996). This study provides insight into the effects nickel has on *S. IU 625* and the response it utilizes to reduce nickel toxicity. The gene *smtA* which has been shown to increase heavy metal resistance was monitored exclusively.

Materials and Methods

Cultures Maintenance

S. IU 625 stock cultures were maintained in an Amerex Instruments Inc., (Lafayette, CA), Gyromax 747R incubator shaker at 26 °C in atmospheric conditions with constant fluorescent light and continuous agitation at 100 rpm. Five ml of cells were inoculated in 95 ml of sterilized Mauro's Modified Medium (3M) in 250 mL Erlenmeyer flasks. The media was adjusted to a pH of 7.9 using 1 M NaOH.

Nickel Chloride Preparation

Stock solution of 1% nickel chloride in dH₂O was prepared using triple distilled water Milli-Q Integral 5 Water Purification System (EMD Millipore, MA) in a sterile container from Sigma Aldrich. The solution was then sterilized by using Millipore 0.45 µm membrane filters.

Growth of *Synechococcus* sp. IU 625 in Nickel Chloride

Various nickel chloride concentrations (0, 10, 25, 50 mg/L) was added to an exponentially growing culture in four 250 mL Erlenmeyer flasks, respectively. Cell growth was monitored through; 1) direct counts via hemacytometer, cells were counted in triplicate for each time point and an average of cell number/square was obtained. The

average was then multiplied by 25 and then 10^4 to obtain the cell number per mL; and 2) turbidity study, optical density (OD) was taken by using a Pharmacia LKB Ultraspec III spectrophotometer at 750 nm wavelength. Cell growth was monitored for 28 days with mean and standard deviations generated through GraphPad Prism.

Microscopic Observation

Aliquots of cells (1 mL) were taken from each time point and used for microscopic analyses. Cells were immediately centrifuged for 1 minute and the supernatant was discarded. Cells were fixed using 5X fixative (12.5% formaldehyde in phosphate buffer). DNA was detected with the use of DAPI (4,6-diamidion-2-phenylindole) fluorescence. Cells were incubated with DAPI (2 $\mu\text{g}/\text{mL}$) for 10 minutes in the dark and placed onto a 1% agarose pad that was pre-made on the slide. Cell morphology was observed using differential contrast with on an Axioscope Lab A1 microscope with Zeiss AxioVision software.

DNA Extraction

Flasks 1-3 were overgrown and needed to be diluted for efficient DNA isolation. Flasks 1, 2, 3 were diluted 1:4 with 1x Tris-EDTA (TE) buffer. Culture 4 was not diluted (1:1). The Norgen protocol kit was followed with the change to incubate at 45 minutes for cell lysis due to thickness of some of the samples. The purity (260/280 ratio) and the

yield (ng/ μ L) of the DNA samples were determined with the Thermo Scientific NanoDrop ND-1000.

Heavy Metal Distribution

Samples were centrifuged immediately after collection and the supernatant placed into a separate microcentrifuge tube. The cell pellet was resuspended in dH₂O. The amount of nickel present in the supernatant and in the cells was determined using ICP-MS protocol by Naturex on an ELAN DRC-E ICP-MS.

Naturex ICP-MS Protocol

Standard Solution Generation

Standard solutions were first generated. The matrix solution was prepared with 20% nitric acid (SCP Science – Nitric Acid, PP, 66-70%, Poly- #250-038-175), 500 ppb gold, 50 ppb internal standard. In a clean squeeze bottle, 300 mL of water was added with 100 mL of nitric acid. 0.25 mL of a gold solution (0.25 mL of 1000 ppm gold solution in 10% HCL) (#N9300212) was added to the nitric acid solution. A multi-element internal standard (2.5 mL of 26 element, 100 mg/L, nitric acid) (#N9303834) was subsequently added to the mixture and diluted with water (SCP Science Blank Water for ICP #140-113-037) to 500 mL. A nickel standard, Perkin Elmer Quality Control Standard 21, (#N9300281) was also used to assess the quantity of nickel.

ICP-MS Acid Digestion

A small aliquot of the sample (0.25 g) was weighed directly in microwavable reactor and nitric acid (10 mL) was slowly added. The solution was cooled by capping and mineralizing. A mineralization sequence was followed (see below). After mineralization, the reaction was cooled to 45 °C and transferred to a 50 mL volumetric flask. A mixture of gold: internal standard (275 µL, 1:1) was added. The flask was then diluted with water (50 mL) and filtered into another 50 mL tube.

ICP Operating Conditions

All basic maintenance was followed before turning on; system was allowed to warm for 15 minutes with the hood and argon flow conditions checked

The following setup was used for an ICP-MS Elan DRC-e, Perkin Elmer with autosampler S10, Perkin Elmer. Microwave accelerated Reaction System, Model (MARSr) with 12 digestion reactors XP1500+ vessel Assembly kits. Power: 1.1 kW, Plasma flow: 15 L/min, Auxiliary flow: 0.95 L/min, Nebulizer flow: 0.93 L/min, Wash time between sample: 45 s, Sample delay: 35 s, Dwell timer per mass: 50 ms, Sweeps per reading: 20, Replicates: 3/Reading per replicate: 1

ICP-MS Sample Analysis

A new dataset was generated by placing blanks, standards and samples into the autosampler. After the samples were generated, the tubing was removed, plasma and argon was turned off. The calibration curve was set according to the following

correlation coefficient limit: 0.995, Curve type: linear, Maximum error %: 15, unit for standards: mg/L or after weight ppm.

RNA Isolation, cDNA Synthesis and qPCR

RNA was extracted from the sample using Trizol Max Bacterial RNA Isolation Kit, Invitrogen. Cells were lysed and RNA separated using phase separation and precipitated out of solution to isolate RNA. RNA was stored in nuclease-free dH₂O. RNA quality and concentration was estimated using a NanoDrop ND-1000.

cDNA was generated using a High Capacity Reverse Transcriptase cDNA kit from Applied Biosystems®. Reactions (10 µL) were conducted with 2 µL buffer (10x), 0.8 µL dNTPs, 2.0 µL RT primers, 1.0 µL RT, and 3.2 µL nuclease-free dH₂O. Reactions were placed on the Applied Biosystems® Veriti® 96-Well Thermal Cycler and followed manufacturer recommendations.

Quantitative PCR (qPCR) was performed with an Applied Biosystems® StepOnePlus Real-Time PCR System. Reactions were set up in triplicate with 6.6 µL nuclease-free water, 1.2 µL each of forward and reverse primer (300 nm) for *smtA*, 10 µL of SYBR green dye, and 1 µL of cDNA (5 ng/µL).

Bioinformatic Analyses

Sequences of known efflux proteins CnrB and AcrB were blasted with BlastP separately against *Synechococcus* species. *Syn.* PCC 7942 and *Syn.* PCC 6301 were found within each BlastP and aligned with a survey of other *Synechococcus* species from the results. A multiple sequence alignment was performed with Muscle5, T-Coffee and Partial Order Alignment (POA). A neighbor-joining phylogenetic tree was generated from the Muscle5 alignments. A conserved sequence region was visualized with Partial Order Alignment Visualizer (POAVIZ).

Results

Growth and Pigmentation Defects

To determine the effects of nickel on the growth of *S.* IU 625 cultures were grown in 3M broth with increasing concentrations of nickel, 0, 10, 25 and 50 mg/L. Previous work has established that these concentrations induce the greatest effect for observation. Cultures were monitored twice a week for 3-4 weeks to demonstrate the complete bacteria growth cycle of lag, log and stationary phases. The growth curves demonstrate that an increase in nickel concentration shows a depression in cell growth up until a certain critical nickel concentration threshold. The 10 mg/L culture was only slightly slower than control initially but quickly rebounded. The 25 mg/L culture had a prolonged lag phase and did not fully enter exponential growth until day 11. The total cell count for the 25 mg/L remained lower than the control and 10 mg/L. The 50 mg/L culture showed little growth and the culture color was pale to clear by the end of the study. A pale color indicates the reduction of cell population or the cells lose

pigmentation. Preliminary data (not shown) establishes that the maximal nickel concentration cells can survive in is lower than 30 mg/L. A study with 30 mg/L culture followed the same trend as the 50 mg/L culture.

A lighter pigmentation of green in the 25 mg/L culture was noted from day 1 to day 8, see figure 2. However the cell number increased slightly in the 25 mg/L during this time, see figure 1. An increase in cell number should darken the green coloring, as seen in the 10 mg/L and 0 mg/L culture. It has been documented that nickel ions can interfere with the electron transfer in the photosystem lowering the fluorescence (Boisvert 2007). This suggests an explanation for the bleaching effect seen in the 25 mg/L during its prolonged lag phase. Further, it may account for the relatively flat Optical Density (OD) change present in the growth curve as pigmentation damage would not fluorescence accordingly.

S. IU 625 Morphological Defects

Increasing concentrations of nickel chloride induced more pronounced morphological defects. Defects present include DNA fragmentation, vibrio shaped cells, and cell size changes. The 10 mg/L nickel chloride culture had an increase in curved cells and cells with ectopic poles, as shown in figure 2. After a week these defects declined rapidly and the cells appeared to have normal morphology and intact DNA similar to that of the control. Higher concentration of NiCl_2 showed similar morphological defects to those observed in the 10 mg/L but were more frequently noted. The 25 mg/L cultures developed morphological defects including abnormal cell morphology and fragmented

DNA. More dead cells (as shown by the lack of DNA) were more frequently present in the 25 mg/L culture than that of the 10 mg/L. After 11 days the cells were capable of growing in the 25 mg/L culture with some minor defects such as vibrio morphology, which remained present throughout the rest of the study. The 50 mg/L culture had an increased prevalence in dead cells and appeared smaller in size. This decrease in size could be in part due to a response to minimize surface area to the hostile environment or a decrease in nutrient intake. By the end of the study, the clear flask color and microscopic observations suggest that a significant portion of cells in the 50 mg/L culture were dead. Figure 3 demonstrates some of the common defects and Figure 4 represents the % cell viability. To calculate the % cell viability, a ratio of dead to alive cells was taken for each respective time-point. Live cells had minimal morphological defects and could be stained with DAPI. Cells that were otherwise considered dead did not stain with DAPI and did not fluoresce under UV light.

Nickel Accumulates Initially within *S. IU 625* but is Virtually Cleared by Day 11

ICP-MS provided data for nickel concentrations in the supernatant and within the cells. Nickel concentrations were normalized against the control. The 10 mg/L culture accumulated 8% more nickel in the cell by day 6 and by day 11 it was reduced to control levels. The 25 mg/L culture accumulated less nickel by day 6 (6%) compared to the 10 mg/L culture. However, the 25 mg/L culture was not fully capable of clearing all the nickel into the supernatant throughout the time-points tested. A 1% increase in nickel concentration was always seen in the 25 mg/L culture over control (figure 5).

Cell Aggregation

Some strains of bacteria such as *E. coli* form biofilms (Perrin 2009). Preliminary data suggests that the portions of the 25 mg/L culture and to a lesser extent the 10 mg/L did aggregate together. Cell aggregation perhaps would minimize the cell's exposure to the environment and increase survivability. Further analysis of cellular aggregation is necessary to verify and determine the exact mechanism.

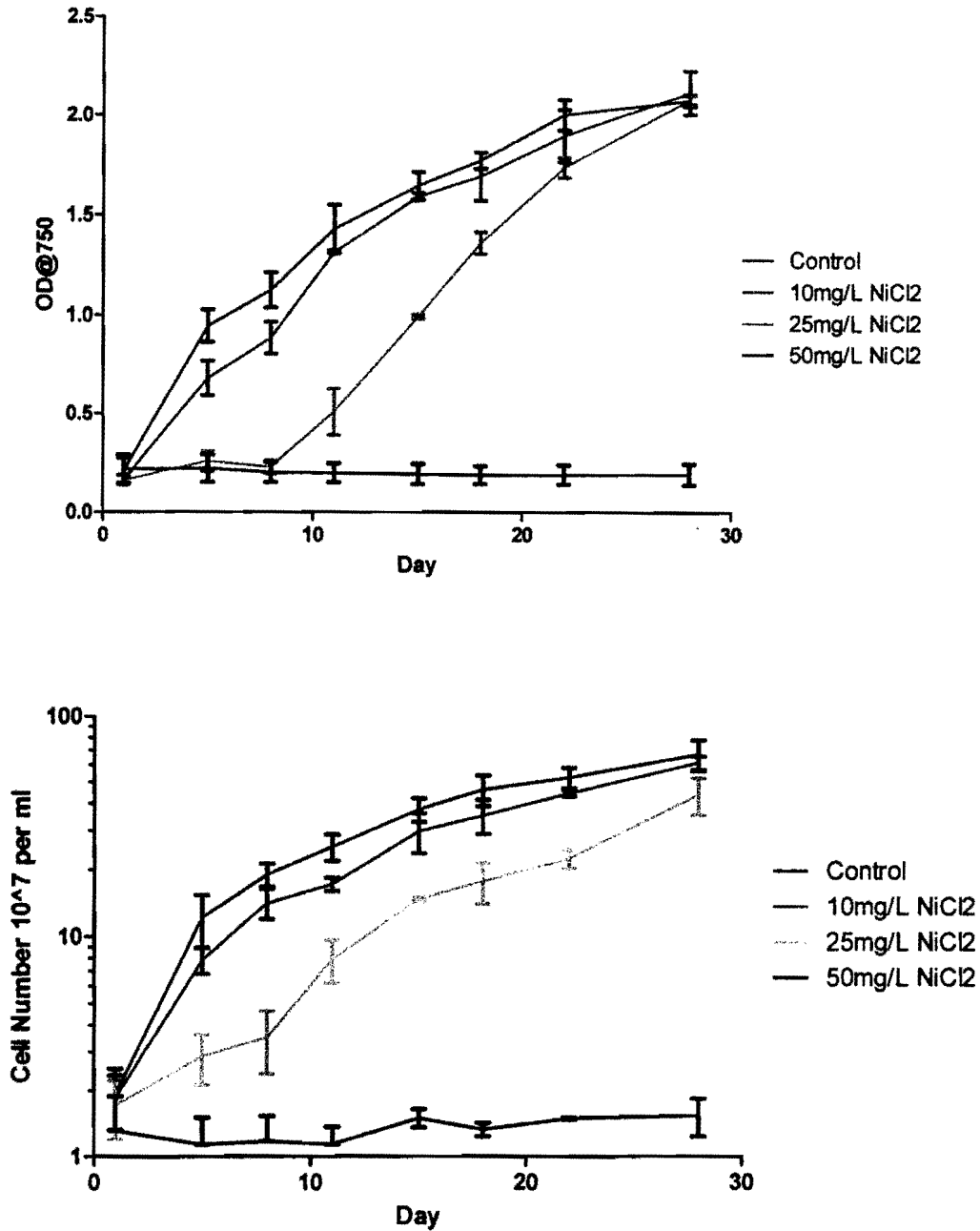


Fig. 1. Growth Curves of *S. IU 625* with or without Nickel Stress: 0 (control), 10, 25 and 50 mg/L NiCl_2 , respectively. Triplicate cultures growth curves were plotted using GraphPad Prism. a) Turbidity study with optical density of each culture plotted over the time course in days. b) Direct count of cultures.

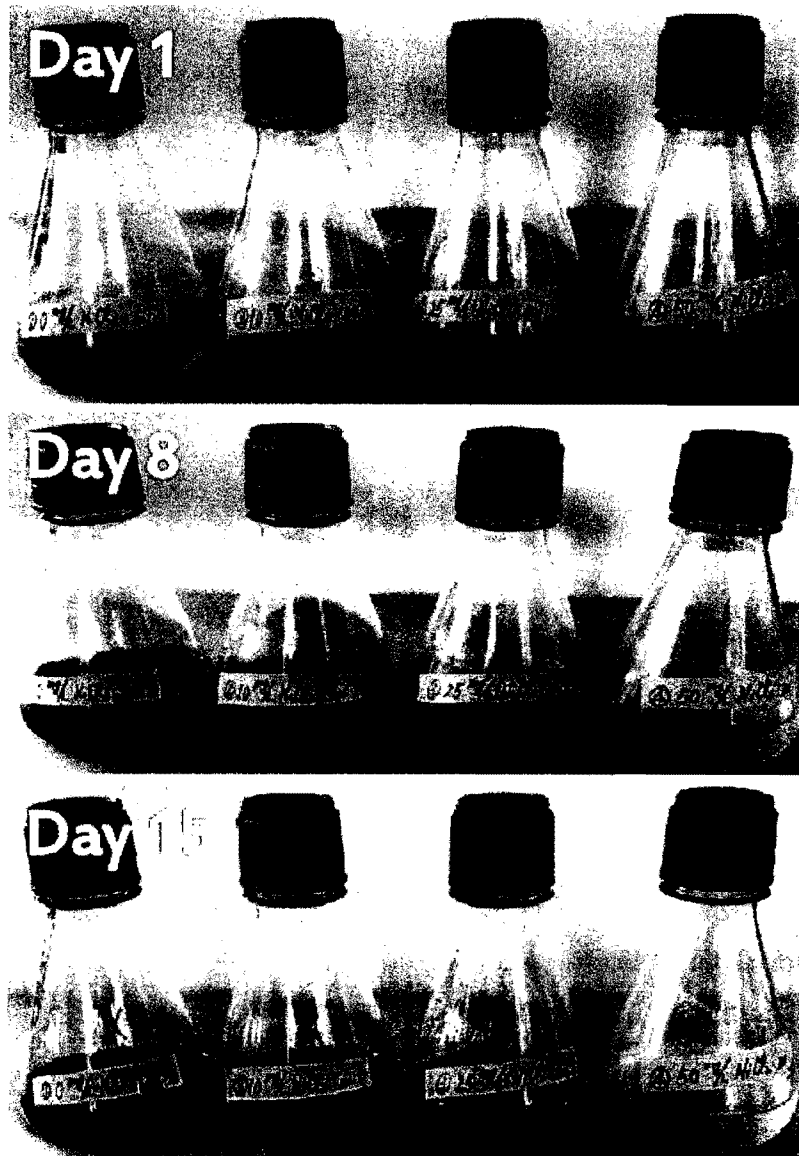


Fig. 2. Pigment Visualization. Left to Right; 0, 10, 25, and 50 mg/L, note the slight discoloration of the 25 mg/L culture on day 8. The color change might be due to free radical nickel ions damaging the pigments. Pictures of flasks were taken each week. Associated day into study is noted in the top left of each picture.

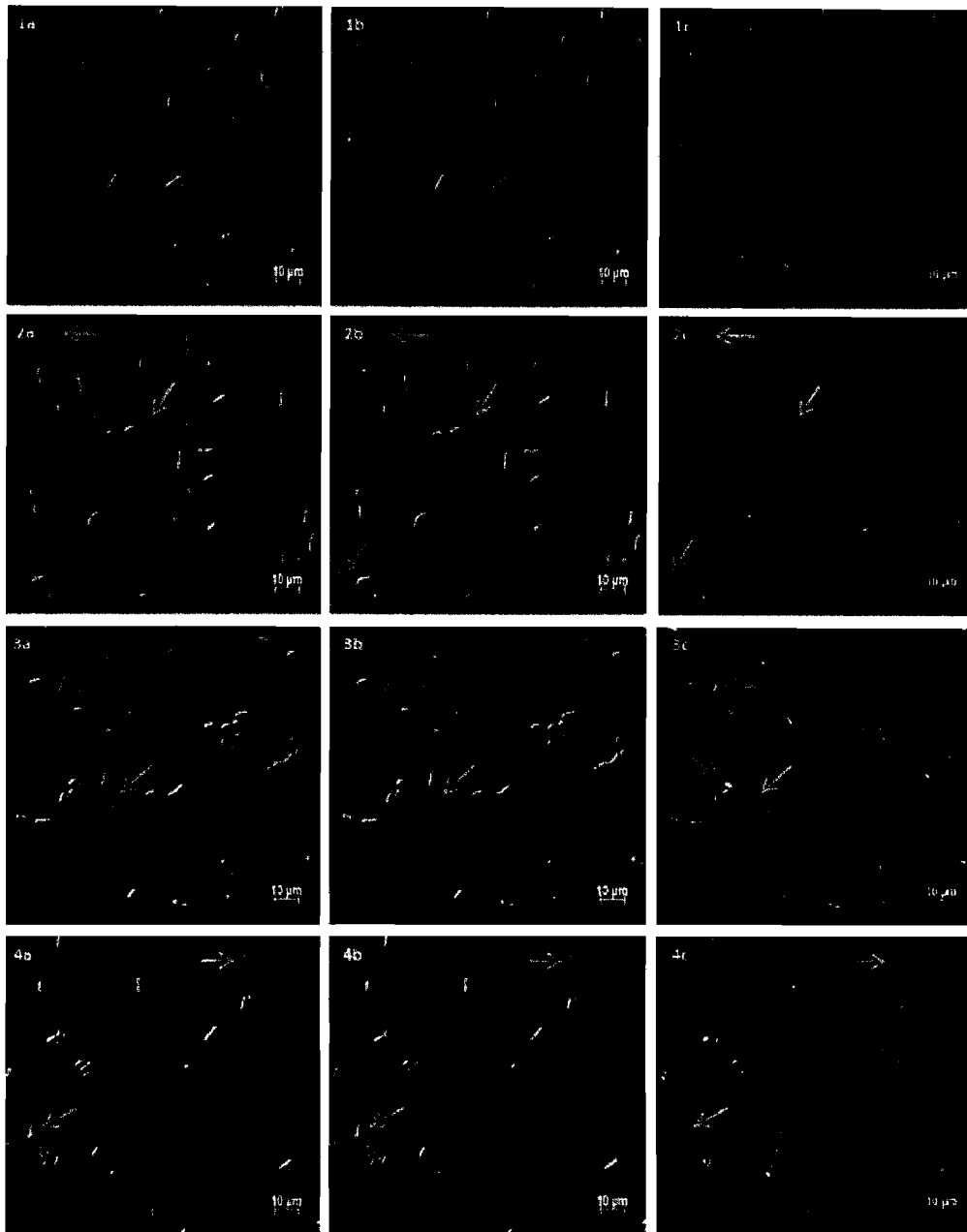


Fig. 3. Microscopic Observations of *S. IU 625* with Various Nickel Concentrations at Day 13. a: overlaid image; b: DIC images; c: DAPI-stained images. 1a-1c: 0 mg/L NiCl₂ (control); 2a-2c: 10 mg/L NiCl₂; 3a-3c: 25 mg/L NiCl₂; 4a-4c: 50 mg/L NiCl₂. Arrows indicate different morphological defects. The same colored arrow indicates the same defect within the culture. Green arrow: normal size cell with no DNA, considered dead; Red arrow: elongated cell may contain DNA; Orange arrow: abnormal morphology, may contain DNA; Purple arrow: Cocci-like, smaller cells, DNA present.

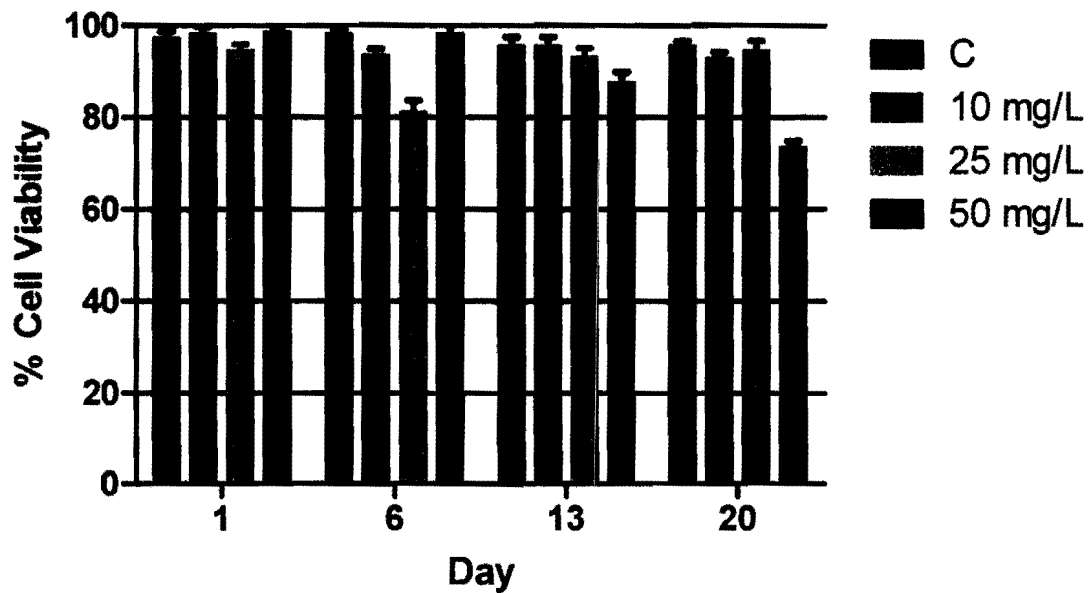


Fig. 4. Cell Viability under Nickel Exposure throughout the Course of the Study. Living cells were considered to have no morphological defects and contained DNA. Dead cells had either a morphology defect or were actually dead and lacked DNA. Percentages of alive cells were calculated and plotted through a 4 week study.

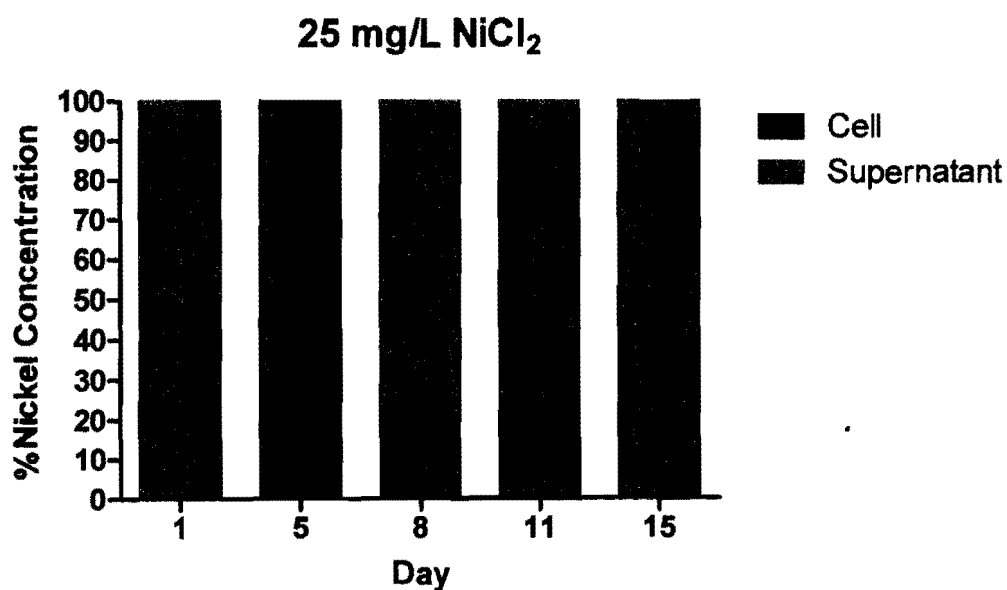
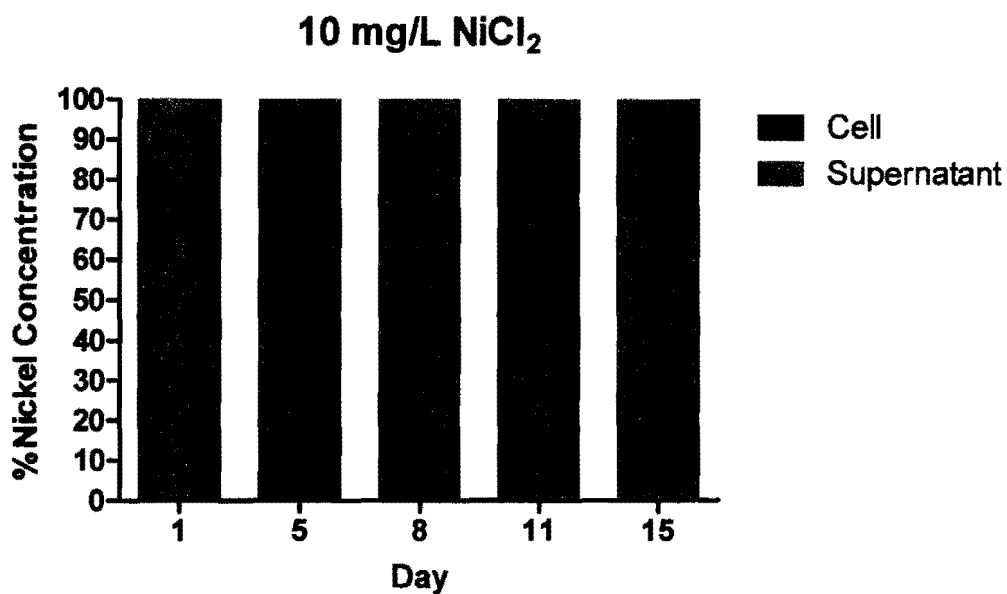


Fig. 5. Distribution of Nickel during the growth of *S. IU 625*. NiCl₂ was initially added to the cells. Nickel dissociates from chloride in an aqueous environment. Raw ICP-MS data was generated examining the nickel concentration against a standard. The raw data was then standardized against the control. The % Nickel Concentration on the y axis represents the increase in nickel over the control.

Metallothionein as a Heavy Metal Response Protein

Metallothionein has been shown to be a heavy metal sequestering protein (Turner 1996). The results of the qPCR data are limited, as only one experiment was performed. Preliminary data indicates that metallothionein may play a role as a nickel response protein in *S. IU 625* (figure 6). The relative quantification data indicates an increase of *smtA* over the housekeeping *rpsL* at day 11 in the culture with 25 mg/L NiCl₂. The 10 mg/L culture remained relatively constant in *smtA* expression levels throughout the study and approximately was always within the standard deviation week to week. The data has been normalized with control and reference samples. Only sample results are shown in the figure 6. The 50 mg/L was not done due to the cell death occurring at such a rapid pace.

The subsequent lower gene expression level of *smtA* in the 10 mg/L compared to control which has no nickel exposure at days 4 and days 11 suggests an alternative mechanism might be at play. Bioinformatic analyses were carried out to better understand the ICP-MS and qPCR results obtained.

Potential Nickel Response Proteins

BlastP results of CnrB and AcrB generated a list of proteins from other strains of *Synechococcus*. The AcrB blast found similarity with *Syn. PCC 7942 HAE1*. HAE1 has been shown to confer a variety of resistances and is a member of the acraflavin family. A multiple sequence alignment with muscle and T-Coffee demonstrated strong homology

with conserved regions. Subsequent neighbor-joining phylogenetic trees were produced with Mega5. The conserved region was visualized with POAVIZ.

Each protein in the survey was approximately 1000 amino acids in length. The conserved region is denoted by the linearity of the sequences in each of the POAVIZ images. The conserved region runs through a significant portion of each protein with some variances in the sequence. This is significant as the phylogenetic tree suggests two different potential functions for the AcrB and CnrB proteins (one being a drug efflux and another being a cation efflux). Multi-drug efflux mechanisms are fairly well established. The strong homology present with the POAVIZ alignment suggests that CnrB might follow a similar mechanism. The variations between CnrB and AcrB are probably due to having a different target substrate for their efflux.

Figure 7 showcases the relationship between genes found in *Syn.* PCC 7942 and *Syn.* PCC 6301 with known CnrB and other cyanobacteria strains. The localization of *Syn.* PCC 7942 and *Syn.* PCC 6301 with the multiple sequence alignment suggest CnrB might play a role in cation efflux.

Figure 8 demonstrates a similar relationship with AcrB. AcrB is an efflux protein that has been shown to confer a variety of resistances. The phylogenetic tree demonstrates a strong homology between *Syn.* PCC 7942 and *Syn.* PCC 6301 across species and suggests a common ancestor. A highly conserved domain was also present.

Figure 9 is a combination phylogenetic analysis of CnrB and AcrB data. The combination tree suggests that each protein confers its own function. The tree is

essentially structured around AcrB and CnrB variants. Subsequent multiple-sequence alignment of all the species' protein demonstrated a strong homology with conserved regions. As the phylogenetic tree suggests a common ancestor might be involved in the development of these two regions of the tree. Ultimately the tree can be divided into two regions based on known function. The AcrB region is potentially a drug resistance branch and the CnrB gene deals with heavy metal or cation efflux. *Syn.* PCC 7942 and *Syn.* PCC 6301 both contain a related family member of each protein in the tree.

S. IU 625 Nickel Response

The expression data of *smtA*, see figure 6, suggests there is an increase in expression levels of 25 mg/L at day 11. The increased expression levels of *smtA* coincide with a decrease in intracellular nickel concentration as seen in the ICP-MS data (figure 5). The 25 mg/L culture at this time was also capable of leaving the extended lag phase and entering the exponential phase as seen in figure 1. *smtA* may have been involved in allowing the cells to start exponential growth at this point. The *smtA* levels coincide with all excess nickel being present in the supernatant at this time. Interesting though, there was no significant up-regulation of *smtA* in the 10 mg/L culture; the levels remained relatively static throughout the study. The *smtA* levels may not have changed drastically in the 10 mg/L culture but the nickel concentration from the ICP-MS data suggests that excess nickel ions were moved into the supernatant, as shown in figure 5. Excess nickel above control was not completely removed until day 11 in the 10 mg/L but this was accomplished a full 3 days earlier in the 25 mg/L at day 8.

The 25 mg/L culture did not fully begin to grow exponentially until after day 11. These observations might mean two potentially different mechanisms are at play. It might be possible that the nickel response mechanism is gauged by cellular sensors and the response is according to the concentration levels (Los 2010). More repeatings are necessary to confirm this trend of gene expression.

The bioinformatic analysis demonstrates a strong homology of a known cation efflux protein, CnrB, with protein from *Syn.* PCC 7942 and *Syn.* PCC 6301. This suggests a potential explanation of the ICP-MS data. The lower expression levels of *smtA* than control for the 10 mg/L culture with nickel still being cleared suggests an alternative mechanism. Efflux proteins present on the membrane can actively pump the heavy metal out. The mechanism is quite similar to that of a multi-drug-efflux protein in which it captures its target, takes it in, and ejects it from the cell. The consensus sequence seen between AcrB and CnrB suggests this mechanism functionality (figure 9). The variation within the consequence sequence could potentially be due to the different substrate binding targets associated with each protein.

Syn. PCC 7942 and *Syn.* PCC 6301 both have family related proteins for AcrB and CnrB within the corresponding phylogenetic trees. Both species contain homologous consequence sequences visualized by POAVIZ, see figures 7, 8. The amino acid length for each protein was approximately 1000. POAVIZ shows a significant portion of the protein length was conserved in *Synechococcus*. A combination of the efflux proteins and SmtA may play a role in nickel resistance.

Combining most efflux proteins with HlyD (usually upstream of efflux proteins) forms a transmembrane efflux operon. HlyD is found upstream of both genes with high homology in *S. elongatus* PCC 7942 and *S. elongatus* PCC 6301. Figure 10 showed the sequence alignment of HlyD suggesting some homology between the two and the operons are proposed (figures 11 and 12). These operons may play a role in nickel efflux.

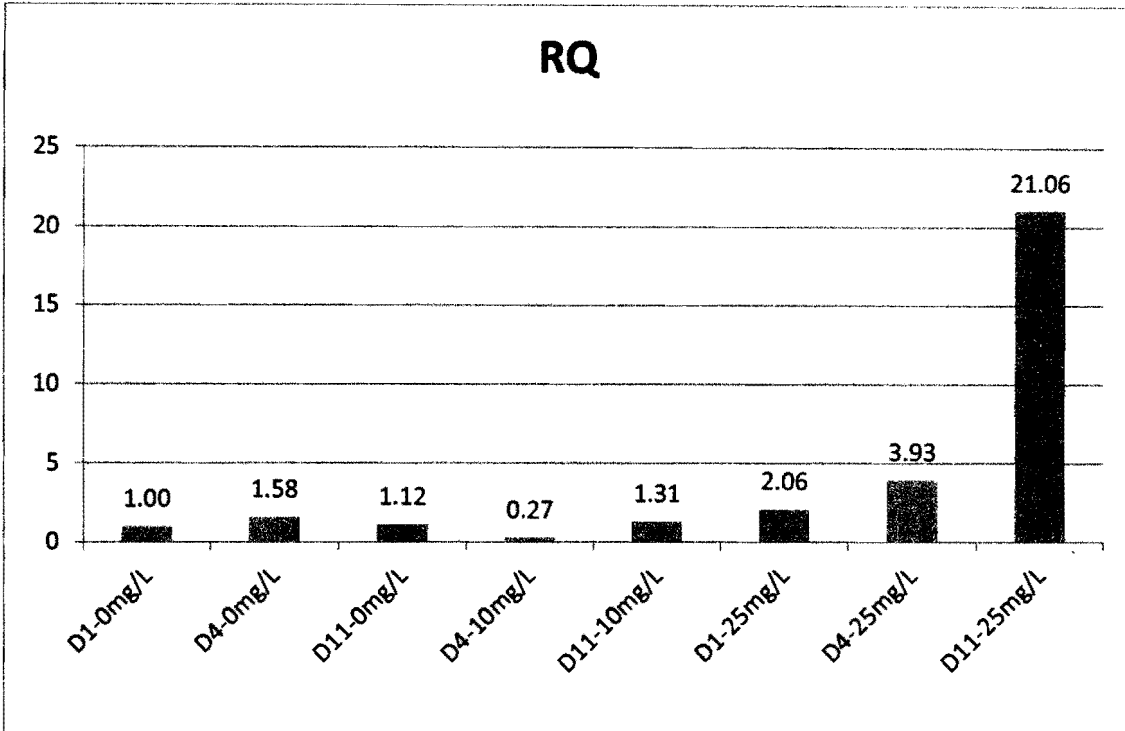


Fig. 6. Relative Quantification of *smtA*. *smtA* expression levels were compared against the internal control, *rpsL*. There does seem to be an increase in gene expression by day 11 (D11) for the 25 mg/L culture. Interesting to note, there was little change in the gene expression for the 10 mg/L. RQ is calculated based on $\Delta\Delta C_T$ (n=3).

```

* Block Label: the length of the sequence
SEQ ID 0: gi1428221553|ref|YP_007105723.1| (HH efflux pump)[Synechococcus sp., PCC 75021]
SEQ ID 1: gi1427723784|ref|YP_0070622406.1| (HH efflux pump)[Synechococcus sp., PCC 63111]
SEQ ID 2: gi1318042452|ref|ZP_07974408.1| (HH efflux pump, CzcR)[Synechococcus sp., CB01011]
SEQ ID 3: gi1352094055|ref|ZP_08955226.1| (HH efflux pump, CzcR)[Synechococcus sp., MH 80161]
SEQ ID 4: gi1113953398|ref|YP_729628.1| (transporter HRE1)[Synechococcus sp., CC93111]
SEQ ID 5: gi1113953398|ref|YP_729628.1| (transporter HRE1)[Synechococcus sp., CC93111]
SEQ ID 6: gi1148242812|ref|YP_001227569.1| (cation efflux)[Synechococcus sp., PCC3971]
SEQ ID 7: gi1254424047|ref|ZP_05037765.1| (RND,HRE1/HRE Family)[Synechococcus sp., PCC 73351]
SEQ ID 8: gi1427714346|ref|YP_007062970.1| (cation/multidrug)[Synechococcus sp., PCC 63121]
SEQ ID 9: gi181301178|ref|YP_401388.1| (HRE1)[Synechococcus elongatus PCC 7942]
SEQ ID 10: gi1113953398|ref|YP_729628.1| (transporter HRE1)[Synechococcus sp., CC93111]
SEQ ID 11: gi1113953398|ref|YP_729628.1| (transporter HRE1)[Synechococcus sp., CC93111]
SEQ ID 12: gi1113953398|ref|YP_729628.1| (transporter HRE1)[Synechococcus sp., CC93111]
SEQ ID 13: gi156751234|ref|YP_172955.1| (cation)[Synechococcus elongatus PCC 6917/942]
SEQ ID 14: gi1113953398|ref|YP_729628.1| (transporter HRE1)[Synechococcus sp., CC93111]

```

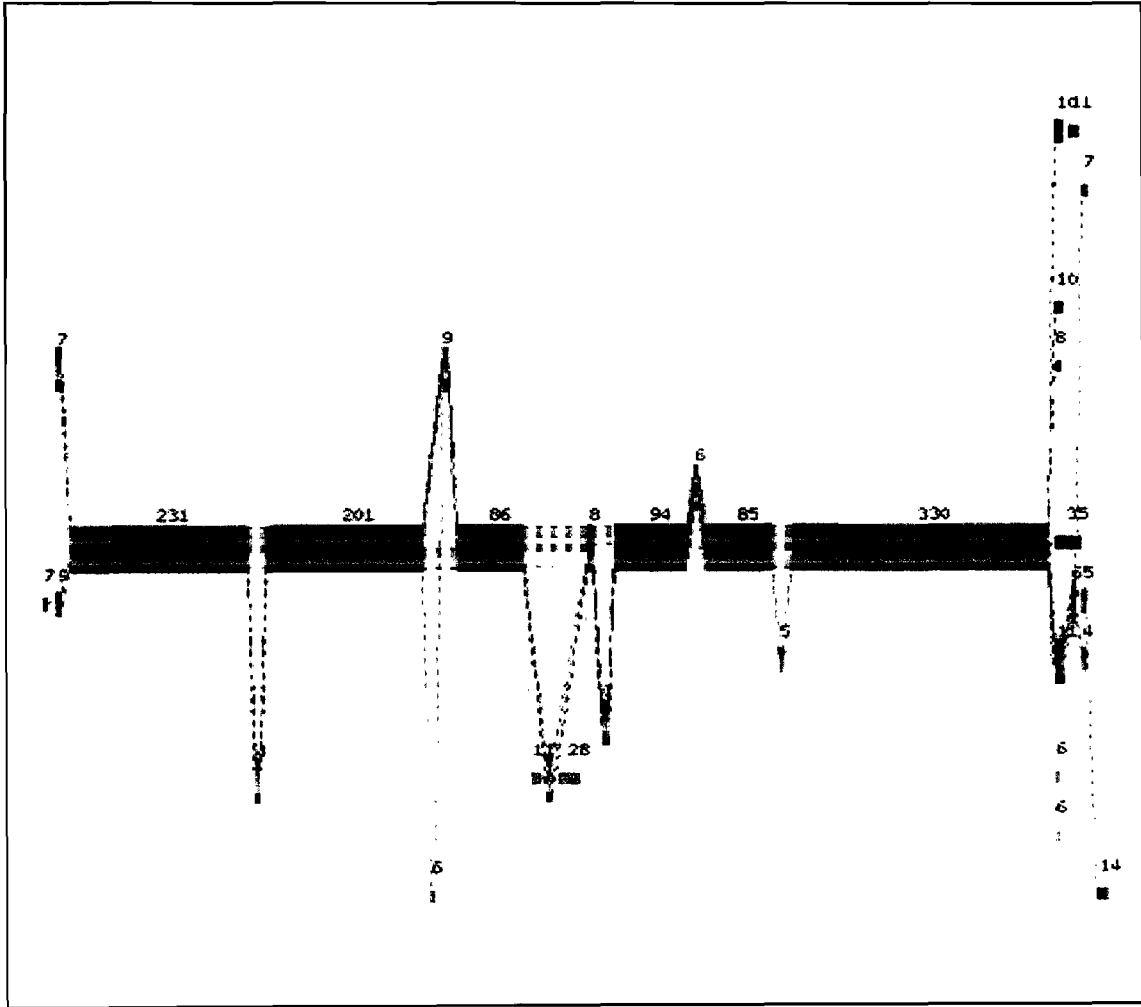


Fig. 7a. Partial Order Alignment of CnrB. POAVIZ was used to visualize the sequence alignment result of 15 *Synechococcus* species. There is strong homology amongst the survey as generated by the linearity of the central region. A cation efflux protein with strong homology was seen in both *Syn.* PCC 7942 and *Syn.* PCC 6301.

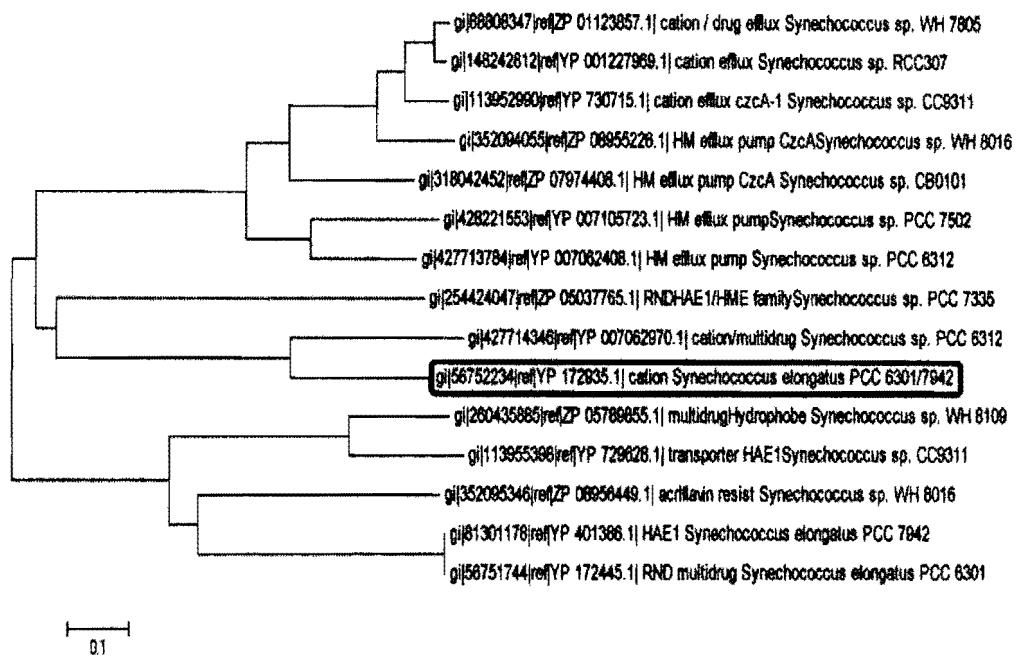


Fig. 7b. Phylogenetic Analysis of CnrB in *Synechococcus*. 15 *Synechococcus* species were chosen via BlastP. Multiple-sequence-alignment was done through Mega5. A neighbor-joining phylogenetic tree was created off this data. Tree demonstrates the relatedness of cation efflux across the species surveyed. Protein results of *Syn.* PCC 7942 and *Syn.* PCC 6301 are in red and located within the heavy metal region of the clades.

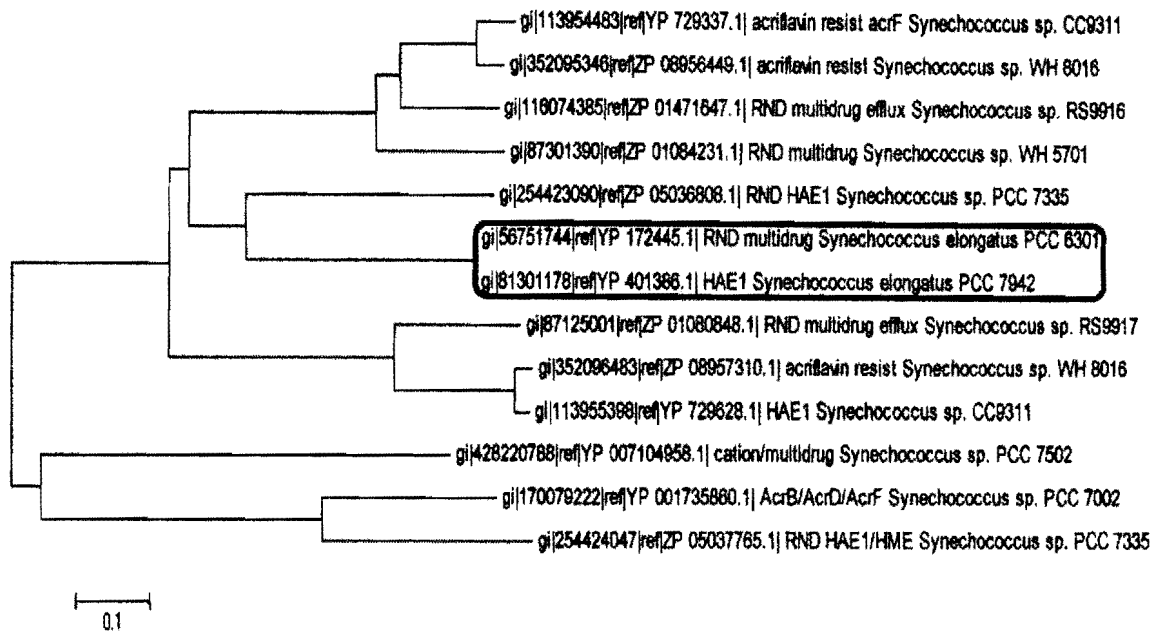


Fig. 8b. Phylogenetic Tree of a known transport protein, AcrB. 13 species of cyanobacteria were chosen via BlastP with AcrB. Multiple-Sequence-Alignment was done with Muscle in Mega5. A neighbor-joining phylogenetic tree was generated from this data. *Syn.* PCC 7942 and *Syn.* PCC 6301 (highlighted) both have high homology and are located within the multidrug resistance bifurcation clade.

SEQ ID 0: gi|428220788|ref|YP_007104958.1 (cation/multidrug [Synechococcus sp. PCC 7502])
 SEQ ID 1: gi|170079222|ref|YP_001735860.1 (AcrB/AcrD/AcrF [Synechococcus sp. PCC 7002])
 SEQ ID 3: gi|56751744|ref|YP_172445.1 (RND multidrug [Synechococcus elongatus PCC 6301])
 SEQ ID 4: gi|81301178|ref|YP_401386.1 (HAE1 [Synechococcus elongatus PCC 7942])
 SEQ ID 22: gi|81301178|ref|YP_401386.1 (HAE1 [Synechococcus elongatus PCC 7942])
 SEQ ID 7: gi|352096483|ref|ZP_08957310.1 (acriflavin resist [Synechococcus sp. WH 8016])
 SEQ ID 10: gi|113955398|ref|YP_729628.1 (HAE1 [Synechococcus sp. CC9311])
 SEQ ID 27: gi|113955398|ref|YP_729628.1 (transporter HAE1[Synechococcus sp. CC9311])
 SEQ ID 25: gi|260435885|ref|ZP_05789855.1 (multidrug,Hydrophobe Synechococcus sp. WH 8109)
 SEQ ID 8: gi|87125001|ref|ZP_01080848.1 (RND multidrug efflux [Synechococcus sp. RS9917])
 SEQ ID 13: gi|428221553|ref|YP_007104958.1 (HM efflux pump[Synechococcus sp. PCC 7502])
 SEQ ID 15: gi|113955398|ref|ZP_08955226.1 (HM efflux pump, CzcA [Synechococcus sp. WH 8016])
 SEQ ID 16: gi|352094055|ref|ZP_08955226.1 (HM efflux pump, CzcA [Synechococcus sp. WH 8016])
 SEQ ID 17: gi|113952990|ref|YP_730715.1 (cation efflux czcA-1 [Synechococcus sp. CC9311])
 SEQ ID 19: gi|148242812|ref|YP_001227969.1 (cation efflux [Synechococcus sp. RCC307])
 SEQ ID 18: gi|88808347|ref|ZP_01123857.1 (cation / drug efflux [Synechococcus sp. WH 7805])
 SEQ ID 14: gi|427713784|ref|YP_007062408.1 (HM efflux pump [Synechococcus sp. PCC 6312])
 SEQ ID 28: CONSENSO (consensus produced by heaviest_bundle, containing 0 seqs)
 SEQ ID 21: gi|427714346|ref|YP_007062970.1 (cation/multidrug [Synechococcus sp. PCC 6312])
 SEQ ID 6: gi|116074385|ref|ZP_01471647.1 (RND multidrug efflux [Synechococcus sp. RS9916])
 SEQ ID 9: gi|116074385|ref|YP_115331.1 (RND multidrug efflux [Synechococcus sp. PCC 7002])
 SEQ ID 11: gi|352095346|ref|ZP_08956449.1 (acriflavin resist [Synechococcus sp. WH 8016])
 SEQ ID 24: gi|352095346|ref|ZP_08956449.1 (acriflavin resist [Synechococcus sp. WH 8016])
 SEQ ID 12: gi|87301390|ref|ZP_01084231.1 (RND multidrug [Synechococcus sp. WH 5701])
 SEQ ID 5: gi|254424047|ref|ZP_05037765.1 (RND, HAE1/HME [Synechococcus sp. PCC 7335])
 SEQ ID 20: gi|254424047|ref|ZP_05037765.1 (RND, HAE1/HME family [Synechococcus sp. PCC 7335])
 SEQ ID 2: gi|254423090|ref|ZP_05036808.1 (RND, HAE1 [Synechococcus sp. PCC 7605])
 SEQ ID 23: gi|81301178|ref|YP_401386.1 (HAE1 [Synechococcus elongatus PCC 7942])

Fig. 9a. *Synechococcus* Species used for POA Analysis. List of species and corresponding protein, CnrB and AcrB used in partial order alignment for combination.

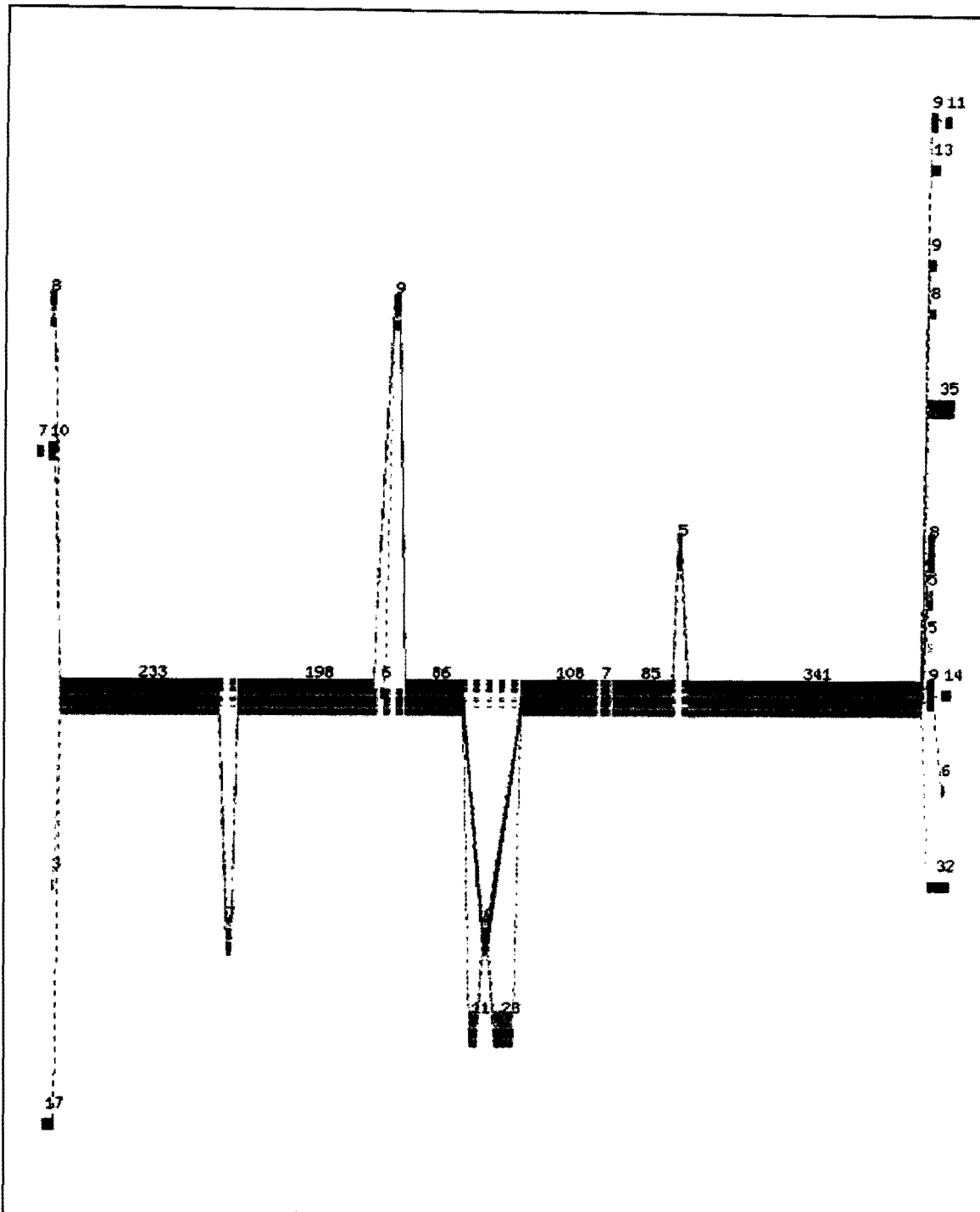


Fig. 9b. Partial Order Alignment of CnrB and AcrB. Both sets of proteins were aligned, this dataset contained 26 species. The image highlights a consequence sequence, visualized by POAVIZ. The linearity of the sequence demonstrates high homology between two different proteins across species surveyed.

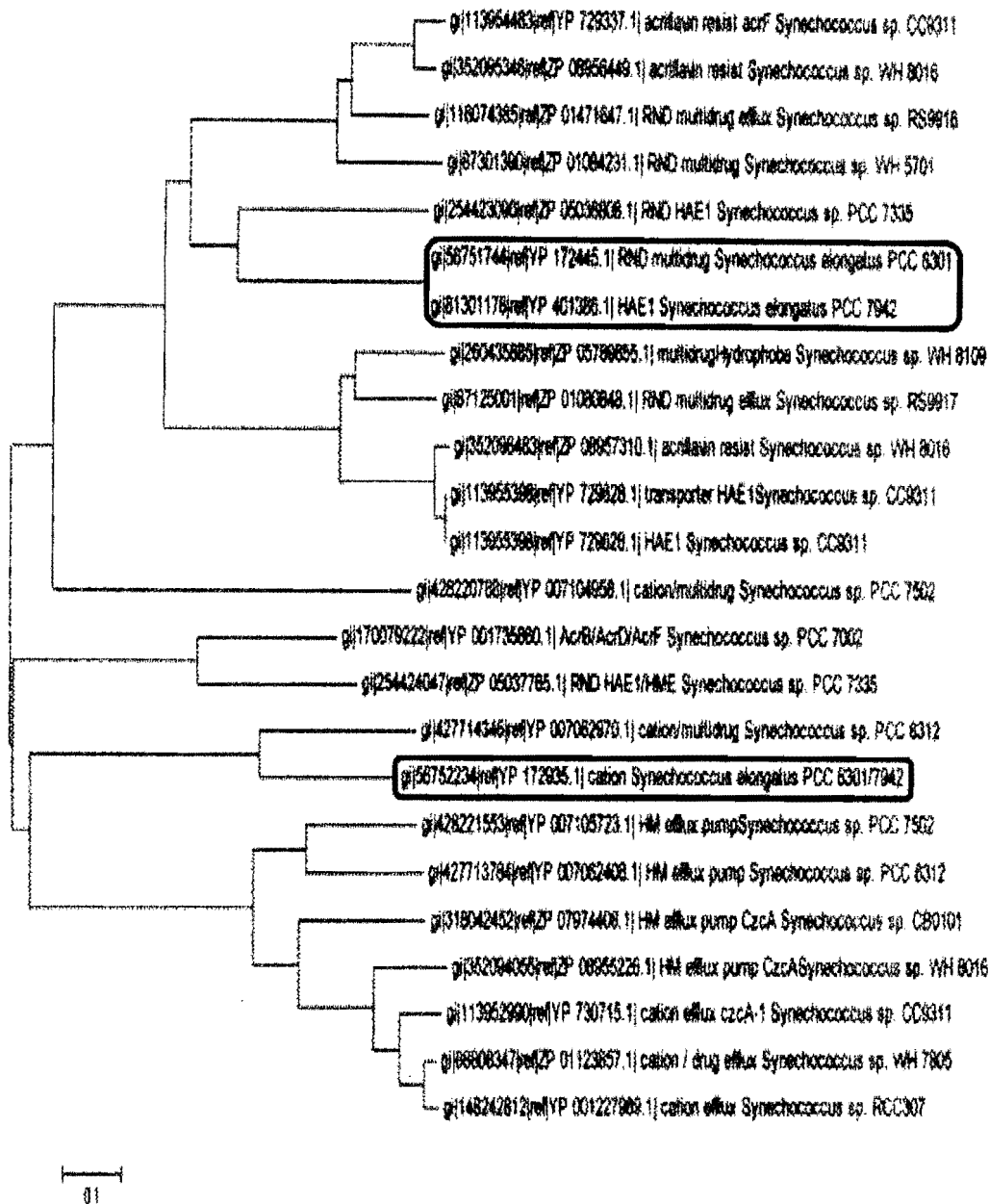


Fig. 9c. Phylogenetic Analysis of CnrB and AcrB. Both sets of CnrB and AcrB data were combined and aligned via Muscle in Mega5. Two different proteins of interest are found in *Syn.* PCC 7942 and *Syn.* PCC 6301. The tree is bifurcated with function being either drug resistance or heavy metal resistance. *Syn.* PCC 7942 and *Syn.* PCC 6301 each have a protein embedded within the branch suggesting function. Both proteins have high homology in their sequence.

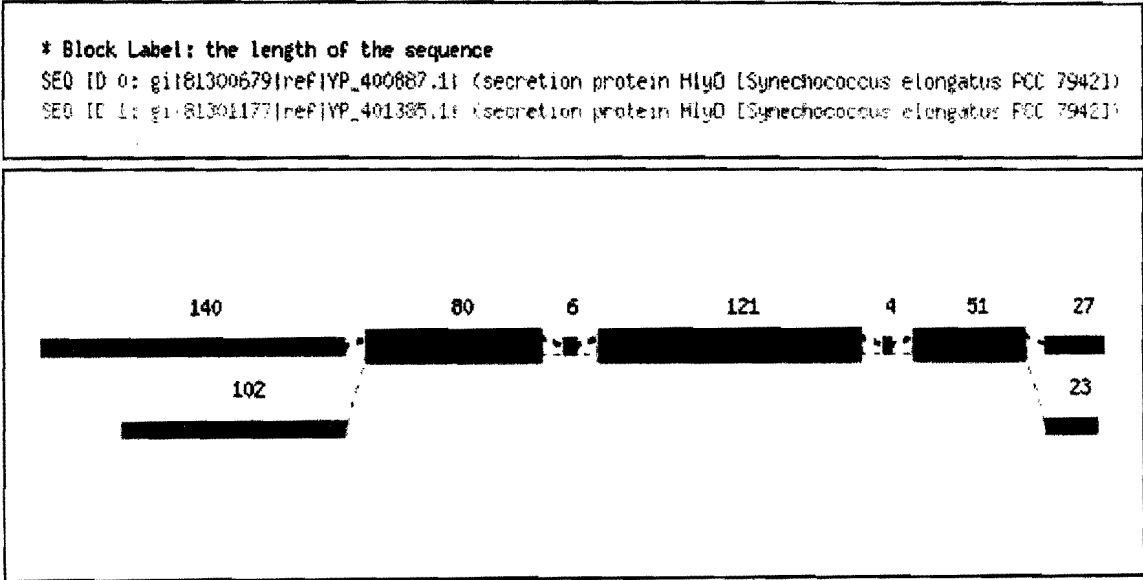


Fig. 10. Partial Order Alignment of hylD. *hylD* is located upstream of both *Syn.* PCC 7942 genes, it is a secretion protein involved in both heavy metal efflux and multi-drug efflux operons.

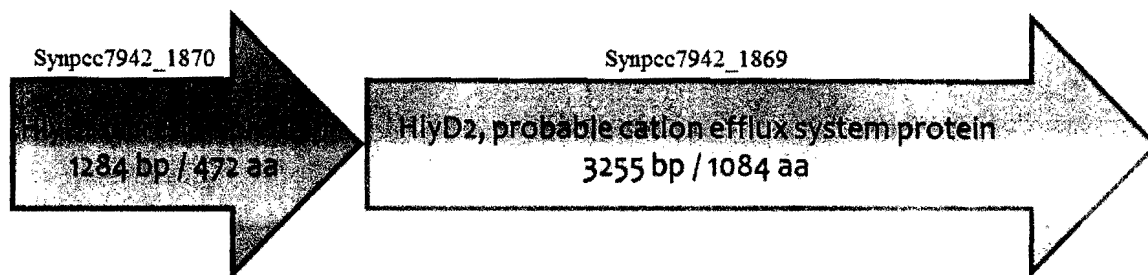


Fig. 11. Potential *nsr* Operon. *hylD* is located upstream of *nsrB/hlyd2*. *hylD* is often associated with efflux genes.

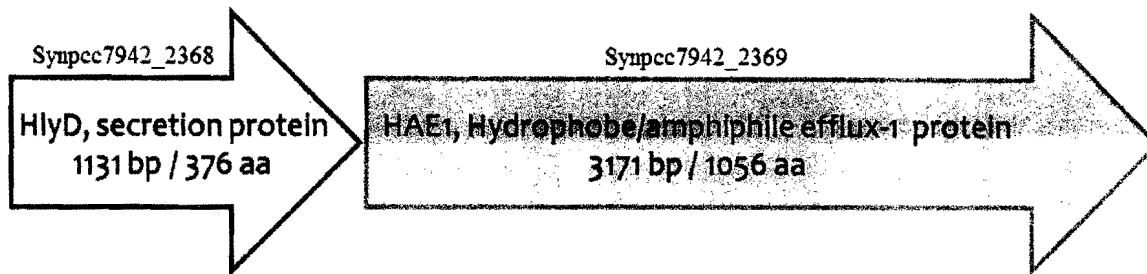


Fig. 12. Potential *hae* Operon. *hylD* is often found upstream of efflux genes. *hylD* is gene Synpcc7942_2368 in the above image, the *HAE1* gene is Synpp7942_2369. The association of *hylD* with an efflux gene constitutes a typical promoter.

Conclusions and Discussion

S. IU 625 demonstrates a remarkable ability to adapt and grow in high nickel concentration conditions. Nickel is normally at “trace” levels in the environment, 0.3 ppb in rivers (Wright 2003). The experiment present here assesses growth that is well above what cells would normally be exposed to. The cells were capable of growing in 10 mg/L and exhibited delayed growth in 25 mg/L. The 50 mg/L was too high a concentration and lead to no growth and eventual death of the culture. Cells at higher concentration of nickel initially accumulated defects at a higher rate. The defects include changes in morphology such as a vibrio-shape, altered cell-size, and fragmented DNA (figure 3). The most notable defect was a bleaching of the cells in the 25 mg/L culture. Bleaching involves a change or loss of coloration in the cells. Figure 2 shows overtime the 25 mg/L culture became a pale green as opposed to a darker green in the control. Interestingly, the corresponding cell number, see figure 1, increased during this timeframe. Together, this suggests potential damage to the pigments normally found in the cyanobacteria. The 25 mg/L culture was capable of fixing the damage and finished the study with a similar dark green coloration to that of the control.

An increase in cell death was also present with higher nickel concentrations. The 50 mg/L had virtually no growth throughout the study. The 10 mg/L had an initial increase in dead cells but returned to levels appreciable to that of 0 mg/L. At day 5 the cell numbers were within a standard deviation between the control and 10 mg/L cultures, both cultures grew increasingly closer in cell number as the study continued on, see figure 1. The 25 mg/L had a drastic increase in dead cells within the first week but by the

end of the second week returned to levels similar to 0 mg/L. The 25 mg/L demonstrated a prolonged lag phase up to day 11 with rapid growth following. The cells also returned to a healthy green color similar to that of the control at this time, see figure 2. The cells were capable of overcoming significant defects to their pigmentation and grew at a rapid rate initially after. Further data provides some insight into understanding this drastic response.

The cell membrane is selectively permeable which allows ions and molecules to cross in and out of the cell. Molecules can be actively transported across the membrane or diffusion can occur through ion channels if a concentration gradient is present. The permeability of the membrane plays an important role in the way nickel crosses the membrane in *S. IU 625* and the cell's response. The ICP-MS data provides an understanding of this process.

The raw data from ICP-MS was standardized against the control levels. Therefore the data present in figure 5 is the % of nickel concentration increase over the control. Cells initially became flushed with nickel. The 10 mg/L culture and 25 mg/L had similar increases in nickel concentration at day 5. Interestingly, this also coincides with the time the 10 mg/L culture was able to leave the extended lag phase and continue growing, see figure 1. At day 8, nickel concentration in the 10 mg/L culture remained higher than the 25 mg/L. The 10 mg/L culture continued to grow despite having elevated nickel levels. By day 11 nickel concentrations within both cultures were similar to that of the 0 mg/L. The 10 mg/L culture had no difference to the 0 mg/L culture and the 25

mg/L had an increase of only 1% nickel. The timeframe between days 11-13 in the 25 mg/L culture seems to be a critical time-point for cellular recovery. The population became stabilized with a reduction in dead cells and an increase in living cells. The 25 mg/L culture began to grow rapidly at day 11, see figure 1, this coincides with the removal of the excess nickel at this time. Cellular pigmentation was recovered around this time in the 25 mg/L culture, see figure 2.

The survival mechanisms for cell survival in this harsh environment kept excess nickel essentially out of the cell. Based on the ICP-MS data only the 50 mg/L culture was overwhelmed with nickel and could not effectively keep the nickel concentration at a survivable level. The 25 mg/L culture did retain some excess nickel throughout the study but that did not impact cell growth after day 11 see figure 1, since the cells grew rapidly after.

The mechanism(s) describing the way *S. IU 625* survives in the increased nickel concentration remains unclear. Noted earlier, cell aggregation was demonstrated in the 25 mg/L culture but not in the 50 mg/L culture. Cell aggregation could potentially minimize exposure to the environment and may play a role in nickel defense. The same 25 mg/L culture that demonstrated cell aggregation on day 13 did not show as a pronounced cell aggregation by day 20. Cell aggregation may slow the intake of nickel. But the ICP-MS data suggests that nickel is still being actively removed from the cells in some way.

Metallothionein is a known heavy metal sequester protein, primarily used for zinc, cobalt, and cadmium defense (Chu 2012). The qPCR data is preliminary and the data is inconclusive. Metallothionein may play a minimal role in nickel response as a long-term defense mechanism. In eukaryotic mice models, metallothionein over-expression did not confer any resistance to nickel-related damage (Wallkes 2004). The qPCR data only examines the response 72+ hours after nickel exposure. The mechanism of metallothionein is that the repressor is removed during high concentrations of heavy metal, primarily zinc.

The proteins and there corresponding genes identified through bioinformatics need to be investigated fully using PCR identification and knock-out studies. Further *smtA* analysis is needed through repeating of long-term studies to clarify the results of the expression levels. Short terms studies, those in which cells have been exposed less than 24 hours, need to be done as well. Analysis short-term study data for ICP-MS and *smtA* will provide a fuller picture of the cellular stress response.

The nickel response mechanism by *S. IU 625* might be multi-faceted encompassing many different proteins at various stages through exposure. Metallothionein may act as a short term response element until the larger, more energy costly, cation efflux proteins are translated and embedded within the membrane. A genomic analysis looking at different genes being active at different times in the study will provide the clearest indication of *S. IU 625* heavy metal response.

More data is necessary to generate any conclusions regarding nickel accumulating on the cell surface and cell aggregation. The mechanism behind the bleaching effect also remains unknown. It is suggested that this effect might be due to pigmentation damaged caused by nickel. But it remains untested experimentally.

More research is needed in this area since pollution is a real world concern that continues to be an increasing problem world-wide. Cyanobacteria have shown there capacity to grow in harmful environments. These strains of bacteria are also capable of leaving behind toxins which can be detrimental to human health. But this is a unique opportunity to study there defense mechanisms and use inactivated forms to fix polluted areas.

Works Cited

- Azeez, P. A. and D. K. Banerjee. "Nickel uptake and toxicity in cyanobacteria." *Toxicological and Environmental Chemistry* (1991): 43-50.
- Banak, Sandra A., Tracie Al. Caller and Elijah W. Stommel. "The Cyanobacteria Derived Toxin Beta-N-Methylamino-L-Alanine and Amyotrophic Lateral Schlerosis." *Toxins* (2010): 2837-2850.
- Boisvert, Steve, et al. "Inhibition of the Oxygen-evolving Complex of Photosystem II and Depletion of Extrinsic Polypeptides by Nickel." *BioMetals* (2007): 879-889.
- Brand, Larry E., et al. "Cyanobacterial Blooms and the Occurance of the neurotoxin beta-N-methylamino-L-alanine (BMAA) in South Florida Aquatic Food Webs." *Harmful Algae* (2010): 620-635.
- Caballero, Hermes Reyes, Gregory C. Campanello and David P. Giedroc. "Metalloregulatory Proteins: Metal Selectivity and Allosteric Switching." *Biophys Chem* (2011): 103-114.
- Cavet, Jennifer S., et al. "A Nickel-Cobalt-sensing ArsR-SmtB Family Repressor." *The Journal of Biological Chemistry* (2002): 38441-38448.
- Chakraborty, Parthasarathi , et al. "Stress and toxicity of biologically important transition metals (Co, Ni, Cu and Zn) on phytoplankton in a tropical freshwater system: An investigation with pigment analysis by HPLC." *Chemosphere* (2010): 548-553.
- Chu, T. C., et al. "Adaptations of Synechococcus sp. IU 625 to Growth in the Prescence of Mercuric Chloride." *Acta Histochemica* (2012): 6-11.
- Chu, T.-C., et al. "Identification of Synechococcus sp. IU 625 metallothionein gene and its evolutionary relationship to the metallothionein gene of other cyanobacteria." *The 2007 International Conference on Bioinformatics & Computational Biology (BIOCOMP 2007)* (2007): 201-207.
- Danilov, Roman A. and Nils G.A. Ekelund. "Effects of Cu²⁺, Ni²⁺, Pb²⁺, Zn²⁺ and pentachlorophenol on photosynthesis and motility in Chlamydomonas reinhardtii in short term exposure experiments." *BMC Ecology* (2001): 1:1.
- Ettinger, Thomas, et al. "Secondary transporters for nickel and cobalt ions: Theme and variations." *BioMetals* (2005): 399-405.

- Foster, Andrew W., et al. "Cytosolic Ni(II) Sensor in Cyanobacterium." *Journal of Biological Chemistry* (2012): 12142-12151.
- Franke, Sylvia, et al. "Molecular Analysis of the Copper-Transporting Efflux System CuSCFBA of *Escherichia coli*." *Journal of Bacteriology* (2003): 3804-3812.
- Garcia-Dominguez, Mario and et al. "A Gene Cluster Involved in Metal Homeostasis in the Cyanobacterium *Synechocystis* sp. Strain PCC 6803." *Journal of Bacteriology* (2000): 1507-1514.
- Gardea-Torresdey, J. L., et al. "Ability of Immobilized cyanobacteria to remove metal ions from solution and demonstration of the presence of metallothionein genes in various strains." *Journal of Hazardous Substance Research* (1998): 2:1-18.
- Hemlata, Tasneem Fatma. "Screening of Cyanobacteria for Phycobiliproteins and Effect of Different Environmental Stress on Its Yield." *Bull Environ Contam Toxicol* (2009): 509-515.
- Lawrence, J. R., et al. "Microscale and Molecular Assessment of Impacts of Nutrients and Oxygen Level on Structure and Function of River Biofilm Communities." *Applied and Environmental Microbiology* (2004): 4326-4339.
- Lee, L. H. and B. Lustigman. "Effect of Barium and Nickel on Growth of *Anacystis nidulans*." *Environmental Contamination and Toxicology* (1996): 985-992.
- Los, Dmitry A., et al. "Stress Sensors and Signal Transducers in Cyanobacteria." *Sensors* (2010): 2386-2415.
- Lustigman, B., L. H. Lee and A. Khalil. "Effects of Nickel and pH on the Growth of *Chlorella vulgaris*." *Environmental Contamination and Toxicology* (1995): 73-80.
- Mishra, Shruti and R. S. Dubey. "Heavy Metal Toxicity Induced Alterations in Photosynthetic Metabolism in Plants." Pessaraki, M. *Handbook of Photosynthesis*. Taylor & Francis Group LLC, 2005. 845-864.
- Perrin, Claire, et al. "Nickel Promotes Biofilm Formation by *Escherichia coli* K-12 Strains That Produce Curli." *Applied and Environmental Microbiology* (2009): 1723-1733.
- Rodionov, Dmitry A., et al. "Comparative and Functional Genomic Analysis of Prokaryote Nickel and Cobalt Uptake Transporters: Evidence for a Novel Group of ATP-Binding Cassette Transporters." *Journal of Bacteriology* (2006): 317-327.

- Schor-Fumbarov, Tamar and Peter B. Goldsbrough. "Characterization and expression of a metallothionein gene in the aquatic fern *Azolla filiculoides* under heavy metal stress." *Planta* (2005): 69-76.
- Tchou-Wong, Kam Meng, et al. "Effects of Nickel Treatment on H3K4 Trimethylation and Gene Expression." *PLoS ONE* (2011): 1-10.
- Tian, Jian, Wu, Ningfend Li, Jian, et al. "Nickel-Resistant Determinant from *Leptospirillum ferriphilum*." *Applied and Environmental Microbiology* (2007): 2364-2368.
- Turner, Jennifer S. "Zn²⁺-sensing by the cyanobacterial metallothionein repressor SmtB: different motifs mediate metal-induced protein–DNA dissociation." *Nucleic Acids Research* (1996): 3714-3721.
- Velikova, Violeta and Tsonko Tsonev. "Changes in photosynthesis, mesophyll conductance to CO₂, and isoprenoid emissions in *Populus nigra* plants exposed to excess nickel." *Environmental Pollution* (2011): 1058-1066.
- Wallkes, Michael P., et al. "Minimal influence of metallothionein over-expression on nickel carcinogenesis in mice." *Toxicology Letters* (2004): 357-364.
- Wang, Bin, et al. "Effects of Cd, Cu, Ni, and Zn on Brown Tide Alga *Aureococcus Anophagefferens* Growth and Metal Accumulation." *Environmental Science and Technology* (2012): 517-524.
- Wright, John. "Heavy metals and pollution of the lithosphere." Wright, John. *Environmental Chemistry*. London: Routledge, 2003. 198-224.
- Zhang, Yan, et al. "Comparative genomic analyses of nickel, cobalt and vitamin B12 utilization." *BMC Genomics* (2009).
- Zhou, Xue, et al. "Effects of Nickel, Chromate, and Arsenate on Histone 3 Lysine Methylation." *Toxicology Applied Pharmacology* (2009): 78-84.